JGR Atmospheres

RESEARCH ARTICLE
10.1029/2024JD041833

Origins of Extreme CAPE Around the World

P. J. Tuckman[1] and **Kerry Emanuel**[1]

[1]Department of Earth, Atmospheric, and Planetary Sciences, Massachusetts Institute of Technology, Cambridge, MA, USA

Key Points:

- Worldwide, accumulation of CAPE is usually caused by surface enthalpy flux mostly through latent heating
- Buildup of CAPE requires a layer of convective inhibition, which in some regions is rare and in others is common
- The CIN accompanying CAPE maxima over water often never decays due to a lack of daytime surface sensible heating

Correspondence to:

P. J. Tuckman,
ptuckman@mit.edu

Citation:

Tuckman, P. J., & Emanuel, K. (2024). Origins of extreme CAPE around the world. *Journal of Geophysical Research: Atmospheres*, *129*, e2024JD041833. https://doi.org/10.1029/2024JD041833

Received 20 JUN 2024
Accepted 8 NOV 2024

Author Contributions:

Conceptualization: P. J. Tuckman, Kerry Emanuel
Data curation: P. J. Tuckman
Formal analysis: P. J. Tuckman
Funding acquisition: Kerry Emanuel
Investigation: P. J. Tuckman
Methodology: P. J. Tuckman
Project administration: Kerry Emanuel
Resources: P. J. Tuckman
Software: P. J. Tuckman
Supervision: Kerry Emanuel
Visualization: P. J. Tuckman
Writing – original draft: P. J. Tuckman
Writing – review & editing: P. J. Tuckman, Kerry Emanuel

Abstract Severe convection, responsible for hazards such as tornadoes, flash floods, and hail, is usually preceded by abundant convective available potential energy (CAPE). In this work, we use a Lagrangian approach to study the buildup of anomalously large values of CAPE from 2012 to 2013 in various regions. Nearly all extreme values of CAPE arise from surface fluxes underneath a layer of convective inhibition (the CIN layer) over several diurnal cycles, but the origin of the CIN layer and the diurnal cycle of surface fluxes differ around the world. In some regions, such as North America and Europe, the air above the boundary layer must be much warmer than usual to form this CIN layer, whereas in other regions, especially the Middle East and central Africa, a CIN layer is common. Additionally, high CAPE occurrences that are over land (those in the Americas, Europe, Africa, and Southeast Asia) tend to lose their CIN layers before the time of maximum CAPE due to large diurnal cycles of sensible heating, whereas those that occur over coastal waters (in the Middle East, Northern Australia, South Asia, and the Mediterranean) usually retain substantial convective inhibition. Uniquely, CAPE in Southeast Australia often builds up due to cooling aloft rather than to boundary layer warming. These results show that one hoping to understand or predict CAPE patterns must understand a variety of mechanisms acting in different regions.

Plain Language Summary The energy available to power severe storms that cause events such as tornadoes and hailstorms is known as convective available potential energy (CAPE). Therefore, these events are usually preceded by the buildup of anomalously large amounts of CAPE. Here, we study the processes by which CAPE accumulates in various parts of the world. In nearly all regions, warming and moistening of near-surface air provides this energy, demonstrating the importance of surface fluxes. However, other characteristics of CAPE accumulation differ around the world, meaning that one hoping to understand how large CAPE values arise must consider specific regions. This work is a step toward understanding where and how frequently severe convective events occur, and if these events will change in the future.

1. Introduction

Severe thunderstorms are among the most dangerous and damaging weather phenomena, producing tornadoes, flash floods, hail, and strong straight-line winds. Societal impacts of these hazards are vast (Changnon, 1999, 2001; Doswell, 2003) and important to understand in the present and future (Botzen et al., 2010; Changnon, 2009). Study of severe convective events uses methods ranging from theoretical and numerical fluid dynamics (Bluestein, 2007; Weisman & Klemp, 1982) to observations of large scale environments (e.g., Carlson & Ludlam, 1968; Yang & Shu, 1985) and has focused on topics including convective initiation by mesoscale processes (e.g., Doswell, 1987; Johnson & Mapes, 2001), the role of soil moisture (Findell & Eltahir, 2003; Ford et al., 2023; Lanicci et al., 1987; Schär et al., 1999; Taylor & Ellis, 2006; Zhang et al., 2023), and the influence of global scale phenomena such as El Niño (Allen et al., 2015; Cook et al., 2017) and climate change (e.g., Botzen et al., 2010; Diffenbaugh et al., 2013; Kunkel et al., 2013; Niall & Walsh, 2005).

The goal of this body of work has largely been to understand the physics and quantify the climatology of severe convective events and estimates exist for worldwide or regional frequencies of tornadoes (H. Brooks et al., 2018; Krocak & Brooks, 2018; Groenemeijer & Kühne, 2014), convective environments (H. E. Brooks et al., 2003; Taszarek, Allen, et al., 2021), and lightning (Kaplan & Lau, 2021). Research often focuses on North America or the continental United States (Grams et al., 2012; Schneider & Dean, 2008; Schultz et al., 2014), where tornadoes tend to be relatively common, but similar work has also studied western and central Europe (Groenemeijer & Kühne, 2014). Global-scale results for this type of work have shown that the most intense thunderstorms on Earth occur in the South-Central United States, southeast South America, and equatorial Africa (Zipser et al., 2006), and that thunderstorm environments are concentrated in equatorial Africa, the central United States, central South America, and near the Himalayas (H. E. Brooks et al., 2003).

How convective events will change with warming has also received attention with results indicating little or unobservable changes with warming of convective events in some regions (Kunkel et al., 2013; Niall & Walsh, 2005) and increases in observed or projected convective events in others (Botzen et al., 2010; Cao, 2008; Diffenbaugh et al., 2013; Gensini & Mote, 2015; Hoogewind et al., 2017). Some of this work has focused on specific aspects of changes with warming, such as nighttime warming (Dessens, 1995) or the strength of updrafts (Del Genio et al., 2007).

One approach to understanding observed and predicted patterns of severe convective events has been to use convective available potential energy (CAPE) or the amount of energy available to be released by convection in a given column of air. CAPE can help illuminate the causes of severe convection (e.g., Chaudhuri, 2012; Murugavel et al., 2014), although severe convection also requires shear and can occur in low-CAPE environments (Sherburn & Parker, 2014). CAPE tends to be largest and most variable in the tropics especially over continents (Riemann-Campe et al., 2009), and the largest CAPE maxima in the world occur over water in the Middle East, the Bay of Bengal, and off the northern coast of Australia (Taszarek, Allen, et al., 2021). Changes in CAPE distributions with warming have also been studied, and an overall increase has been predicted and observed with warming with significant regional variations (Chen & Dai, 2023; Chen et al., 2020; Romps et al., 2014).

Lastly, there has been some work on how CAPE builds up in the time before individual events (Agard & Emanuel, 2017). It has been shown that convective inhibition (CIN), or a layer of warm air above the boundary layer, is necessary for the buildup of high CAPE (Carlson et al., 1983), as a "CIN layer" allows for the accumulation of energy in the boundary layer without this energy being drained by convection (although convection does not always occur when CIN disappears, which may allow further increases in CAPE). Local soil and vegetation properties play a vital role throughout this process, as surface fluxes impact the creation of a CIN layer and the accumulation of moisture below that layer (Agard & Emanuel, 2017; Emanuel, 2023; Zhang et al., 2023). In North America, for example, high CAPE accumulates due to differential advection of anomalously warm air over a moist surface, forming a CIN layer under which moisture accumulates for one or two diurnal cycles (Tuckman et al., 2023).

In this paper, we study how CAPE builds up around the world. Reanalysis data are used to track relevant air parcels backwards from times of large CAPE and observe how these parcels change over time. We characterize CAPE buildup using four factors: (a) the amount of CIN during the diurnal cycle before the time of peak CAPE, (b) the proportion of potential energy increase due to boundary layer warming rather than to cooling aloft, (c) how much warmer the CIN layer is than usual for that area and altitude, and (d) the relative magnitude of the diurnal cycle of surface fluxes over the day before the time of maximum CAPE. We find that in most regions, the largest CAPE maxima occur when CAPE builds up over several diurnal cycles. This CAPE buildup is dominated by surface heating in almost every region studied (except southeast Australia), and most regions require anomalously warm air above the boundary layer to allow this buildup. However, some regions, such as the Middle East and northern tropical Africa, have a constant supply of warm air from nearby deserts, creating a near constant CIN layer. The CIN layer can be broken by strong daytime sensible heating when the CAPE maximum is over land, but this does not occur when it is over water. These results highlight the need to study severe convective events by region.

The rest of this paper is organized as follows. Section 2 discusses the data analyzed and the methods used to track air parcels, identify CAPE maxima in regions of interest, and understand how properties of the relevant air change over time. Section 3 presents and discusses three examples of high CAPE occurrences and then shows composites of different categories of CAPE buildup, followed by a discussion of how CAPE buildup differs around the world. Section 4 discusses these results, their implications, and possible avenues of future research, then the Appendix A shows the accuracy of convective properties calculated from ERA5 reanalysis for a few case studies.

2. Methods

2.1. Data Used

All data shown are from ERA5 global reanalysis (Hersbach et al., 2020) obtained at https://cds.climate.copernicus.eu/. We analyze hourly data on 0.25° resolution from 2012 to 2013 and use multi-linear interpolation, (i.e., a polynomial linear in all four coordinates fit to the surrounding data points) if values not on a grid point are needed. A time period of 2 years is chosen so as to maximize the number of CAPE peaks while keeping the amount of data

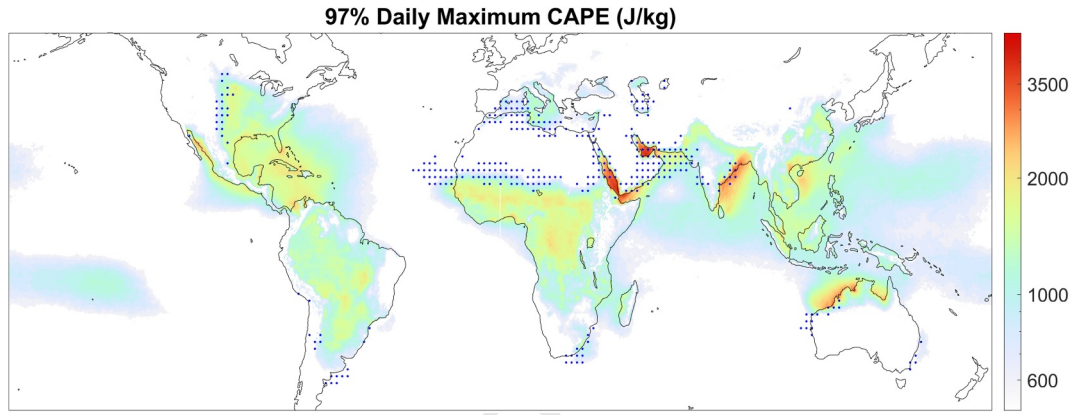

Figure 1. The spatial distribution of high CAPE occurrences. Color indicates the 97th percentile of daily maximum CAPE, or the threshold of CAPE which is exceeded roughly once per month at each location. The blue dots indicate regions in which the average CIN when CAPE exceeds this threshold is at least 75 (J/kg).

manageable. Reanalysis is not perfect and may have systematic biases when calculating energetic quantities (Gensini et al., 2014; Taszarek, Pilguj, et al., 2021; Taszarek et al., 2018). However, there is precedent for using reanalysis to study convective events (H. E. Brooks, 2009; H. E. Brooks et al., 2003; Meukaleuni et al., 2015; Taszarek, Allen, et al., 2021; Tuckman et al., 2023; Westermayer et al., 2017), and ERA5 has been shown to be the most accurate reanalysis for the study of CAPE (Taszarek, Pilguj, et al., 2021). We discuss using reanalysis data and compare ERA5 to observed soundings for a few cases in Appendix A. We find ERA5 to be sufficiently accurate to be useful in most of the world, but we also show that reanalysis may have large errors in equatorial Africa and therefore exclude the region from this study.

2.2. Identifying High CAPE Occurrences

We begin our study by identifying high CAPE occurrences in various regions. To do so, the hourly CAPE at each horizontal grid point in 2012 and 2013 is calculated from reanalysis data by reversibly lifting a near-surface parcel through the column above it and integrating the resulting buoyancy difference with respect to pressure. This is given mathematically as

$$\mathrm{CAPE} = -R_d \int_{p_0}^{p_{\mathrm{LNB}}} (T_{vp} - T_{ve})\, d \log p \tag{1}$$

where R_d is the ideal gas constant of dry air, p is pressure, p_0 is the original pressure of the lifted parcel, p_{LNB} is the level of neutral buoyancy (usually near the tropopause), T_{vp} is the virtual temperature of the lifted parcel, and T_{ve} is the virtual temperature of the environment. The lifted parcel is chosen to originate 25 hPa above the surface so as to be representative of the mixed layer, and parcel properties are calculated at this level via linear interpolation. We also define CIN, or Convective Inhibition, as the same integral evaluated from p_0 to the level of free convection. We refer to this as the "CIN layer," and in it the buoyancy of the lifted parcel is negative, so CIN represents the barrier to convection being initiated. Note that CAPE and CIN are defined only when there is at least one pressure level where the lifted parcel is positively buoyant with respect to the surrounding air, that is, $T_{vp} > T_{ve}$ for some value of p.

Next, we identify what "high CAPE" corresponds to at each horizontal grid point by calculating the 97th percentile of daily maximum CAPE at that grid point. The result of this calculation is shown in Figure 1 and indicates where the highest values of CAPE on Earth occur. Although the 97th percentile is chosen arbitrarily, the map is similar to previous work that used the 95th percentile (Taszarek, Allen, et al., 2021), indicating that the qualitative results do not depend on the value chosen. The largest values of CAPE worldwide (>2.5 kJ/kg) appear in the Persian Gulf, the Red Sea, the western edge of the Bay of Bengal, and off the northern coast of Australia. Other moderately high CAPE values occur in equatorial Africa, East Asia and just off the coasts of East Asia, central North America, the Gulf of Mexico, and South America.

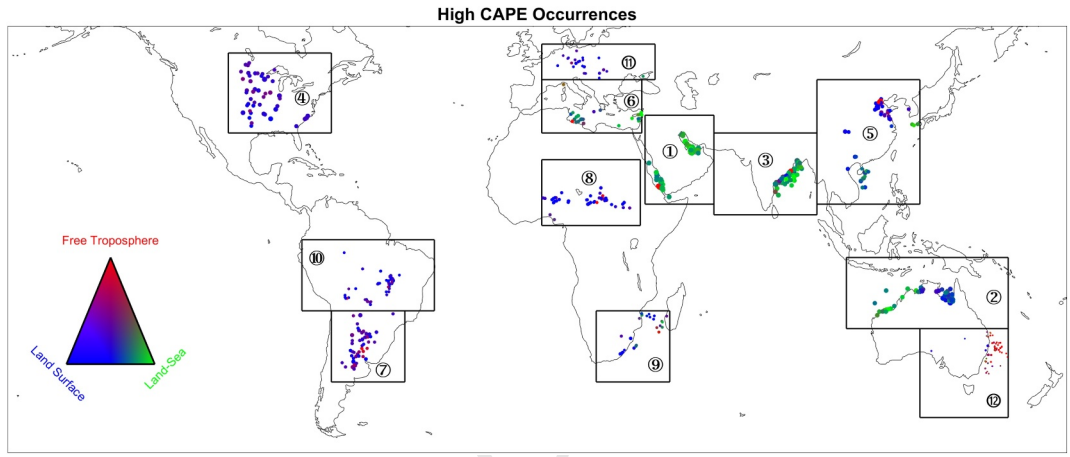

Figure 2. The maxima identified for study (points) in selected regions (boxes, numbers corresponding to the list above). The size of each point corresponds to the amount of CAPE, whereas the color corresponds to the physical cause of high CAPE, with red indicating troposphere cooling and blue (green) indicating a large (small) surface flux diurnal cycle. Quantitative definitions of these values and explanations of their importance are in the following sections. Boxes in this figure indicate where CAPE peaks were found, regions searched extend across North America (area 4 began at 130°W) and Asia (area 3 extends to 60°N).

To understand whether these extreme CAPE values will lead to severe weather, we are also interested in the CIN at the time of high CAPE. Even if a near-surface parcel is positively buoyant with respect to much of the free troposphere (i.e., CAPE is large), if there is a strong enough CIN layer, severe convection is unlikely to occur. Therefore, Figure 1 also displays which areas have an average of 75 (J/kg) or greater CIN when the daily maximum CAPE is above the 97th percentile. We see that the Mediterranean, the southern Sahara, the Middle East, the Bay of Bengal, northern Australia, and the western edge of the high CAPE region of North America all have substantial CIN when CAPE is large, indicating that severe weather is unlikely to occur.

Based on the CAPE and CIN patterns shown in Figure 1, along with common locations of severe convective events and our analysis of the reliability of reanalysis data (see Appendix A, we believe reanalysis in Equatorial Africa may be unreliable), 12 regions are selected to study (listed in order of median CAPE):

1. Middle East
2. Northern Australia
3. South Asia
4. North America
5. Southeast (S.E.) Asia
6. Mediterranean
7. Southern South America (S.A.)
8. Africa
9. Southern Africa
10. Tropical South America (S.A.)
11. Europe
12. Southeast (S.E.) Australia

and identify high CAPE occurrences in each region by the following process. First, the CAPE data are smoothed via a simple moving mean with a window of 1.25° longitude, 1.25° latitude, and 3 hr. Then, all local maxima in three dimensions (longitude, latitude, and time) are identified, and the largest of these in each region are chosen for study. Fifty CAPE maxima are identified in most regions, whereas 25 are identified in southern Africa, Europe, and the Mediterranean. This number of maxima is chosen as a balance between computational limitations and having enough maxima to compute meaningful statistics. Figure 2 shows the regions studied, the locations of CAPE maxima, and aspects of their physical causes. The three types of CAPE peaks are defined in the following sections.

2.3. Lagrangian Tracking

Once high CAPE occurrences are identified, we utilize a Lagrangian trajectory approach to study the buildup of CAPE and the time evolution of relevant quantities. For each CAPE maximum, we select 13 boundary layer parcels (those with the most CAPE) within two degrees of the latitude and longitude of maximum CAPE, and we track those parcels by integrating the eastward, northward, and vertical velocities backwards using a 15 min time step (with velocities interpolated from hourly data). Several parcels are used to minimize noise, and trajectories are followed for up to 72 hr before the time of maximum CAPE. Once a CIN layer is identified (see next section), the same procedure is applied to the parcels that end up there. We do not track parcels of the free troposphere that end up above the surface parcels, as changes to the free troposphere are rarely important to the buildup of CAPE (shown in Tuckman et al. (2023) and throughout this work).

2.4. Quantities Studied

To study the buildup of CAPE, we calculate several properties of the relevant air parcels. The basic quantities are the temperature (T), specific humidity (q), and geopotential height (z) of each parcel and the vertical column above it (hereafter, the "seen" column), and these are used to calculate composite quantities. This above parcel profile is referred to as the "seen" column as it is what the parcel sees above it as it moves. Additionally, the evaporation and sensible heat flux from the surface are recorded at the horizontal position of the tracked parcel.

Using the basic quantities, we calculate the virtual potential temperature (θ_V) of each air parcel and the column above it (seen θ_V) as well as the θ_V of the tracked parcel lifted adiabatically into that column. The difference between this "lifted θ_V" and the seen θ_V is referred to as $\Delta\theta_V$ and is a measure of the buoyancy the tracked parcel would have at a given height. Below the pressure of the tracked parcel, $\Delta\theta_V$ is defined to be zero.

Although CAPE and CIN are useful quantities, they are vertically integrated and often difficult to interpret, so we define PCAPE and PCIN as more understandable proxies. PCAPE represents an energy difference between a boundary layer parcel and the free troposphere, so that it is related to the integrand of CAPE. Specifically

$$\text{PCAPE} = \text{MSE}_{\text{b.l.}} - \text{MSE}^{*}_{\text{500hPa}} \tag{2}$$

where the (saturated) moist static energy $\text{MSE}^{(*)}$ is defined as

$$\text{MSE}^{(*)} = Lq^{(*)} + c_p T + gz \tag{3}$$

where $L = 2.25 \times 10^6$ (J/kg) is the latent heat of vaporization of water, $c_p = 1005$ J/(kg K) is the specific heat of air at constant pressure, $g = 9.8$ m/s^2 is the acceleration due to gravity, and q^* is the saturated specific humidity. The saturated MSE is used as it is a basis for comparison against the surface parcel if that parcel were lifted into the free troposphere, where it would be saturated. The MSE^* is evaluated at 500 hPa so as to be representative of the free troposphere.

PCIN, meanwhile, is defined as the most negative $\Delta\theta_V$ between 600 and 900 hPa, so it is a measure of negative buoyancy where the boundary layer parcel is most negatively buoyant. If a boundary layer parcel were to ascend, it would have to pass through this layer, and PCIN is a metric of how much additional energy it would need to do so. Air representative of the CIN layer is also tracked backwards, and these are chosen as originating above the boundary layer parcels at the pressure and time of maximum negative buoyancy.

PCAPE and PCIN are useful as we can separate the buildup of CAPE or CIN into a contribution from changes in the boundary layer (i.e., $\text{MSE}_{\text{b.l.}}$ or lifted θ_V) and a contribution from the column above the boundary layer (i.e., the $\text{MSE}^{*}_{\text{500hPa}}$ or seen θ_V).

Lastly, we would like to determine if the properties of the CIN layer differ from their long term averages. Therefore, we define a monthly mean θ_V as the column θ_V at the position and time of day of the largest PCIN averaged over the month in which a CAPE maximum takes place.

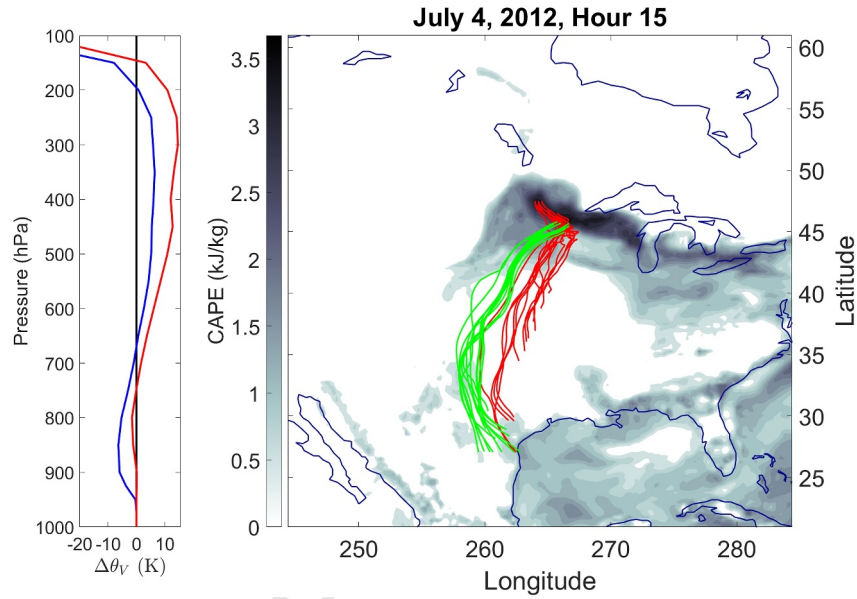

Figure 3. Introduction to the first CAPE maximum example. The main panel shows the trajectories of the boundary layer parcels leading up to the time of maximum CAPE (red) and the parcels that form the CIN layer at the time of maximum PCIN (green), both displayed for the 60 hr before the time of maximum CAPE as well as the spatial distribution of CAPE at the time of maximum CAPE. The left panel shows the vertical profile of the virtual potential temperature difference averaged over the tracked boundary layer parcels at the time of maximum PCIN (blue) and the time of maximum CAPE (red). The title indicates the day and approximate local sun time of the CAPE maximum.

3. Results

In this section, we present results on how anomalously large CAPE episodes occur. We begin with three examples, then show composites of three types of high CAPE occurrences, and finally present statistics on how CAPE builds up differently in various regions of the world.

3.1. Examples

Our first example high CAPE episode, introduced in Figure 3, is typical of those in central North America and similar to many studied by Tuckman et al. (2023). This CAPE maximum occurred just west of the Great Lakes region on 4 July 2012 at roughly 3 p.m. local sun time, and the region of large CAPE (about 3 kJ/kg) stretches from ∼260° longitude to Lake Superior and spans a few degrees latitude (main panel of Figure 3). The vertical profile of $\Delta\theta_V$ (left panel) at the time of maximum CAPE is roughly as expected, being zero in the boundary layer (>950 hPa), slightly negative but essentially zero for a small layer above that (between 925 and 750 hPa) and large and positive for remainder of the troposphere (between 750 and 150 hPa). The vertical profile of $\Delta\theta_V$ at the time of max PCIN, on the other hand, has a significant CIN layer (i.e., layer of negative $\Delta\theta_V$) from 700 to 950 hPa and much less positive area in the free troposphere. The boundary layer parcels at the time of maximum CAPE had been near the Gulf of Mexico 60 hr before the time of maximum CAPE and moved continuously north with a small amount of zonal movement (red lines, main panel). The parcels that end up in the CIN layer also came from the south but from further west over drier soils (green lines).

We now seek to understand the cause of this CAPE maximum by studying how relevant quantities changed in the days before the time of maximum CAPE (Figure 4). The CAPE following the boundary layer parcels (Figure 4a) increased significantly on the day of maximum CAPE, starting around sunrise, but there was also substantial CAPE (1–2 kJ/kg) the day before. There was over 300 J/kg of CIN both the night before the time of maximum CAPE (−9 hr) and the night before that (−33 hr). The vertical structure of the relevant energetic quantities (i.e., $\Delta\theta_V$) as a function of pressure and time is shown in Figure 4b. The buildup of CAPE (red area) occurred beginning at around −30 hr and reached from 700 hPa to the top of the troposphere. By examining the seen θ_V, that is, the θ_V profile at the horizontal position of the boundary layer parcels, we can separate the CAPE time series into a component from boundary layer changes and a component from changes aloft. The seen θ_V contours are mostly

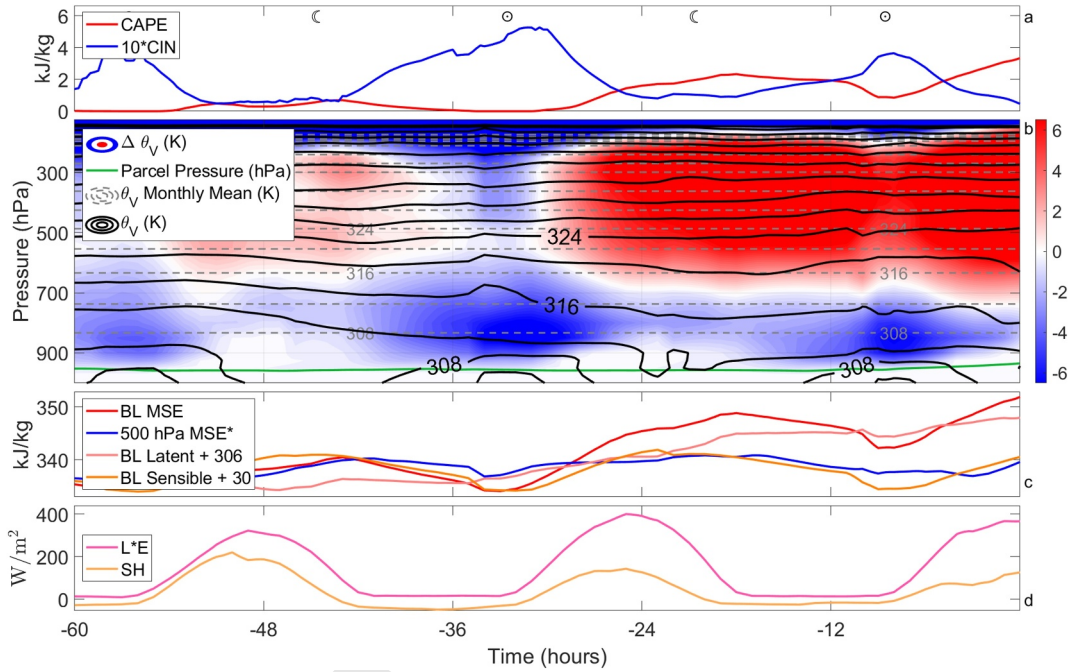

Figure 4. Relevant quantities over time for the first example of a high CAPE episode. Panel (a) shows the CAPE and CIN with the CIN scaled by a factor of 5. Note that each quantity is averaged over the parcels tracked, and that they are not defined if a parcel is negatively buoyant with respect to its entire column. In these cases, the CIN of that parcel is ignored and CAPE is set to zero, and the average is taken over the remaining parcels. The sun and moon symbols at the top of the panel indicate approximately 6 a.m. and 6 p.m. local time. Panel (b) shows the virtual potential temperature difference ($\Delta\theta_V$) between the lifted boundary layer parcels and the column above it (color), the virtual potential temperature (θ_V) of this column (solid contours, contour interval 4 K, shown up to 364 K), and the monthly averaged θ_V in the region of the boundary layer parcels when the CIN layer was strongest, all as a function of time and pressure. The tracked parcel pressure over time is indicated by a green line. Panel (c) shows the relevant quantities for the buildup of PCAPE; boundary layer MSE (red), divided into sensible energy (orange) and latent energy (pink), and the 500 hPa MSE* (blue). Sensible and Latent energy are adjusted by constant values so that they fit on the same axis as the full MSE. Panel (d) shows the evaporation (pink, scaled by the latent heat of vaporization) and surface sensible heat flux (orange) at the horizontal location of the boundary layer parcels.

horizontal above 600 hPa (e.g., the 324 K line), indicating constant seen θ_V, and therefore that buildup of CAPE is not a result of changes to the free troposphere. We can quantitatively measure the importance of boundary layer processes for CAPE buildup using PCAPE, that is, comparing changes in the boundary layer MSE to changes in 500 hPa MSE* (Figure 4c). Over the two days before the time of maximum CAPE, the boundary layer MSE has a strong diurnal cycle and increases significantly (by ∼15 kJ/kg), whereas the 500 hPa MSE* barely changes. This indicates that PCAPE builds up due to changes in the boundary layer not changes aloft.

The CIN, meanwhile, is represented by regions of negative $\Delta\theta_V$ between 900 and 750 hPa in Figure 4b. The change in CIN over the several days before the time of maximum CAPE is mostly due to processes above the boundary layer, as the 312 K line of seen θ_V moves down starting from around −54 hr. This indicates an increase in 800 hPa temperature, which increases CIN, as it will be harder for the boundary layer parcel to be lighter than this air. The diurnal cycle of CIN, on the other hand, is controlled mostly by the surface parcels, as on each day, the 316 and 312 K contours are mostly flat. In order to understand how this day of high CAPE differs from ordinary days, we examine the average nearby θ_V profile averaged over the month in which the CAPE maximum occurs at the time of day of maximum PCIN. The upper troposphere during this event is similar to its monthly mean with the 324 K contours lining up almost perfectly in the last 12 hr, whereas the lower free troposphere is much warmer than usual. Specifically, the air of the CIN layer (blue region the night before maximum CAPE) seems to be about 4 K (one contour) warmer than the monthly mean. This indicates that the CIN layer air during the buildup of CAPE (−30 to 0 hr) is anomalously warm for the region.

As the CAPE buildup is due to an increase in boundary layer MSE, we can divide that increase into a latent energy component (i.e., Lq, Figure 4c) and a sensible energy component ($c_pT + gz$). We see that most of the diurnal

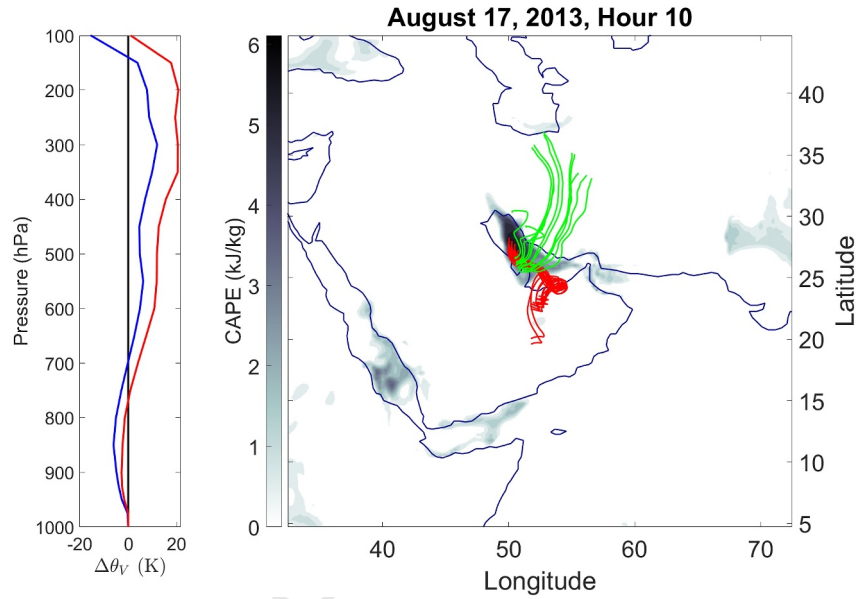

Figure 5. Same as Figure 3 but for the second example of a high CAPE episode.

cycle is coming from the sensible component, whereas the overall increase in low level MSE is coming from the latent component. In this Lagrangian analysis, advection is implicitly included, so it is likely that changes in energy come from the surface (Figure 4d). Both evaporation and sensible surface fluxes have very strong diurnal cycles, which generally correspond to the large increases in MSE. The decreases in sensible energy occur at night, when the sensible surface flux is small or negative and the air parcels are cooling through longwave radiation emission. Although the overall buildup of boundary layer energy is dominated by evaporation, the surface sensible heating is essential to the decrease of CIN on the day of maximum CAPE. In other words, the buildup of moisture increases CAPE and PCAPE, but it is the daytime surface sensible heating starting from −9 hr that leads to CIN decreasing from ∼300 (J/kg) to near zero.

To summarize the first example, CAPE accumulates over the 2 days before the time of maximum CAPE due to a monotonic increase in boundary layer latent energy. Processes in the free troposphere are not directly important for the buildup of CAPE, but the CIN which precedes CAPE is due to the formation of a CIN layer, which is 4 K warmer than the long time mean for the area. This CIN allows MSE to build up underneath it without the CAPE being used by convection. Then, the CIN layer disappears just before the time of maximum CAPE due to daytime sensible heating. All of this is in agreement with Tuckman et al. (2023), where it is shown that these features are typical for large CAPE values over North America. We label this type of CAPE maximum as "land surface CAPE" due to the importance of surface fluxes and their diurnal cycles over land, and other maxima of this type are shown as blue dots in Figure 2.

Our second example high CAPE occurrence happened over the Persian Gulf on 17 August 2013 at 10 a.m. local time (Figure 5). The region of high CAPE covers most of the Persian Gulf and has CAPE values of up to 6 (kJ/kg). However, the vertical profile of $\Delta\theta_V$ at the time of maximum CAPE (left panel) shows that there is still CIN at this time, likely preventing convection. The boundary layer parcels mostly arrived at the area of high CAPE from nearby land, but they had been over the Persian Gulf for some time. In contrast, the parcels which make up the CIN layer came directly from elevated land just a few hours before.

The time evolution of the relevant quantities for this second example are shown in Figure 6. CAPE begins to increase in the final 36 hr (Figure 6a), but there is CIN above the boundary layer parcels going back to at least 25 hr before that. The CIN is remarkably constant over this time; its diurnal cycle is small due to the large heat capacity of the Persian Gulf. By looking at the vertical structure of $\Delta\theta_V$ and the background θ_V, we see that the small increase in CIN the night before the CAPE maximum matches closely with a warming of the region between 700 and 850 hPa, demonstrated by the 320 K line moving down. However, the monthly mean θ_V profile indicates that the air, which forms the CIN layer is only 2 K warmer than usual (compared to 4 K in the first example). It is

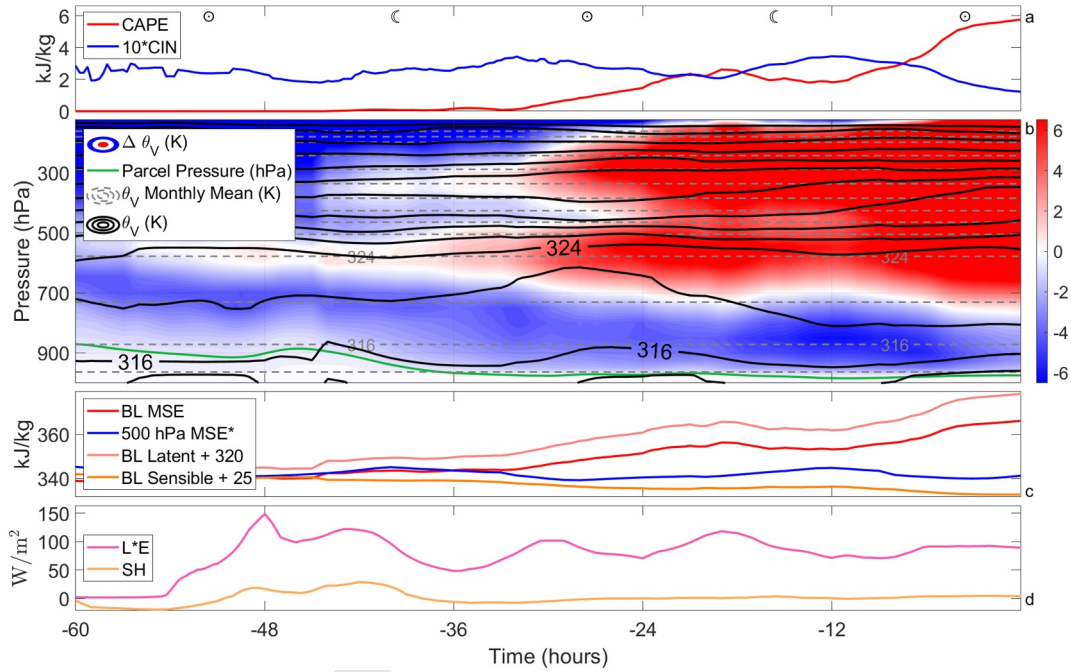

Figure 6. Same as Figure 4 but for the second example of a high CAPE episode.

likely that hot desert air from the surrounding regions is often advected over the cool moist surface of the Persian Gulf, leading to a consistently strong CIN layer. Meanwhile, CAPE builds up due to increasing $\Delta\theta_V$ above this layer, reaching from 700 hPa to the top of the troposphere. This CAPE increase is not controlled by the free troposphere; the θ_V contours in the upper troposphere are mostly flat. Additionally, the seen 500 hPa MSE* does not change significantly for the 60 hr before the time of maximum CAPE (blue line, Figure 6c) just as in the first example. However, the buildup of boundary layer MSE has a different character here than in the first example; the boundary layer sensible energy is almost completely constant, having no diurnal cycle. The latent energy increases monotonically and significantly as dry boundary layer air moistens over the Gulf, although the rate at which it is increasing has a small diurnal cycle. Both these features match the surface fluxes at the position of the boundary layer parcels, where there is strong evaporation and very little sensible heating starting from around −56 hr. In other words, the dry and warm air that has moved over the Persian Gulf (at −56 hr) is receiving energy through evaporation but little or no sensible heat from the cool and wet surface. The resulting large increase in humidity without sensible heating leads to a very unstable profile (i.e., high values of CAPE), but there is no way for the boundary layer to become warm enough to overcome the CIN layer created from the surrounding desert air.

To summarize, a relatively cool moist surface adjacent to a hot dry surface can lead to high CAPE and CIN by air from the dry surface being advected over the moist surface. The hot dry air will form a layer of large θ_V (i.e., a CIN layer), which cannot be overcome due to a lack of daytime sensible heat from the surface, but the buildup of humidity in the boundary layer will mean that the column is unstable to deep convection and have significant CAPE. It is likely that the extraordinarily high CAPE arises simply from boundary layer parcels remaining over water for a significant amount of time (∼48 hr, visible in Figure 6d). The longer a parcel is over water, the more its relative humidity will increase without its temperature changing, leading to large CAPE even if evaporation is not anomalously large. As the contrast between the cool, wet water surface, and the nearby hot, dry land is vital for this mechanism, we label this type of high CAPE occurrence "land-sea CAPE," and similar peaks are shown as green dots in Figure 2.

Our final example CAPE maximum occurred on 19 September 2013 off the coast of Eastern Australia at roughly midnight local sun time (Figure 7). There was significantly less CAPE in this example than the others, at most 2 (kJ/kg), there was very little CIN at the time of maximum CAPE (left panel), and little CIN at the time of maximum PCIN the night before. The boundary layer parcels arrived at the location of maximum CAPE from the

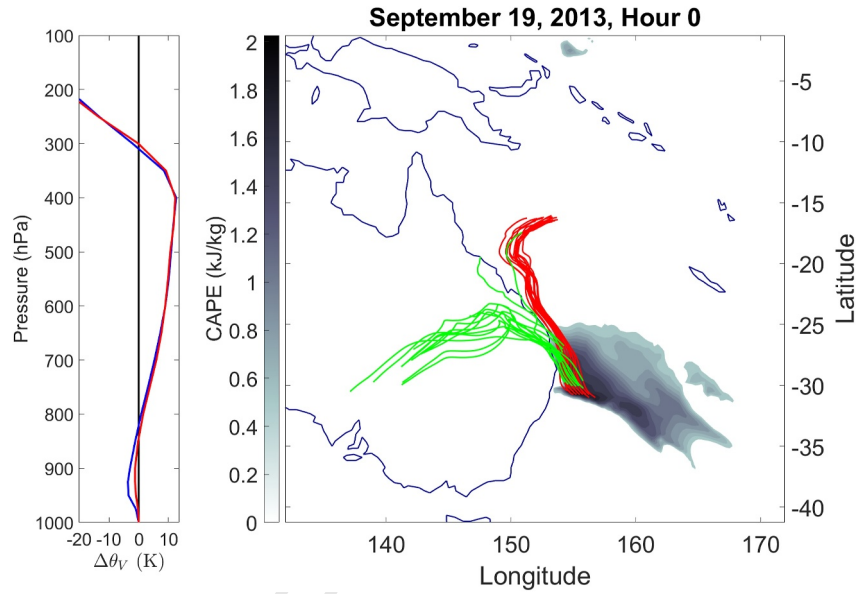

Figure 7. Same as Figure 3 but for the third example of a high CAPE episode.

north, having been over water for at least 60 hr before the event, whereas the CIN layer parcels arrived from the West, where they were over land (i.e., Australia).

Figure 8 shows the time evolution of relevant quantities for this high CAPE occurrence. The CAPE builds up over the 24 hr before the time of maximum CAPE but not due to the normal diurnal cycle, as the maximum CAPE is at midnight. There is some CIN in the area of the boundary layer parcels going all the way back to 48 hr before the time of maximum CAPE, but the CIN decreases quickly in the last few hours. We see how this case differs from the others based on the vertical structure of θ_V (Figure 8b). Although $\Delta\theta_V$ looks as it does in the other cases with a layer of CIN around 900 hPa and a larger layer of positive buoyancy from 800 to 300 hPa, the θ_V profiles are quite

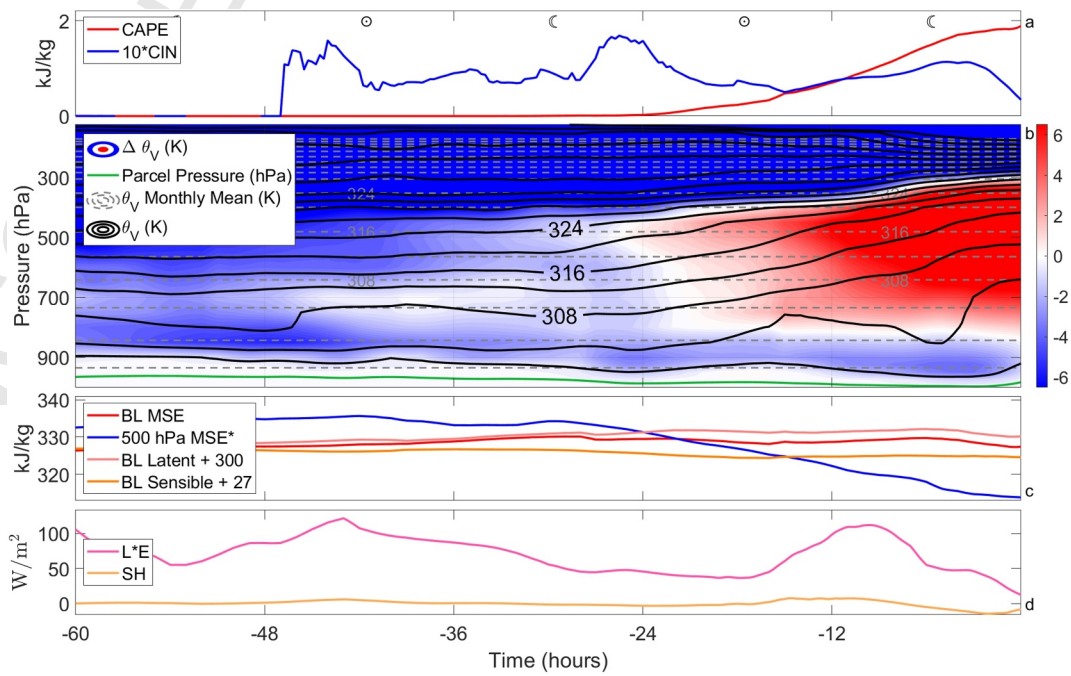

Figure 8. Same as Figure 4 but for the third example of a high CAPE episode.

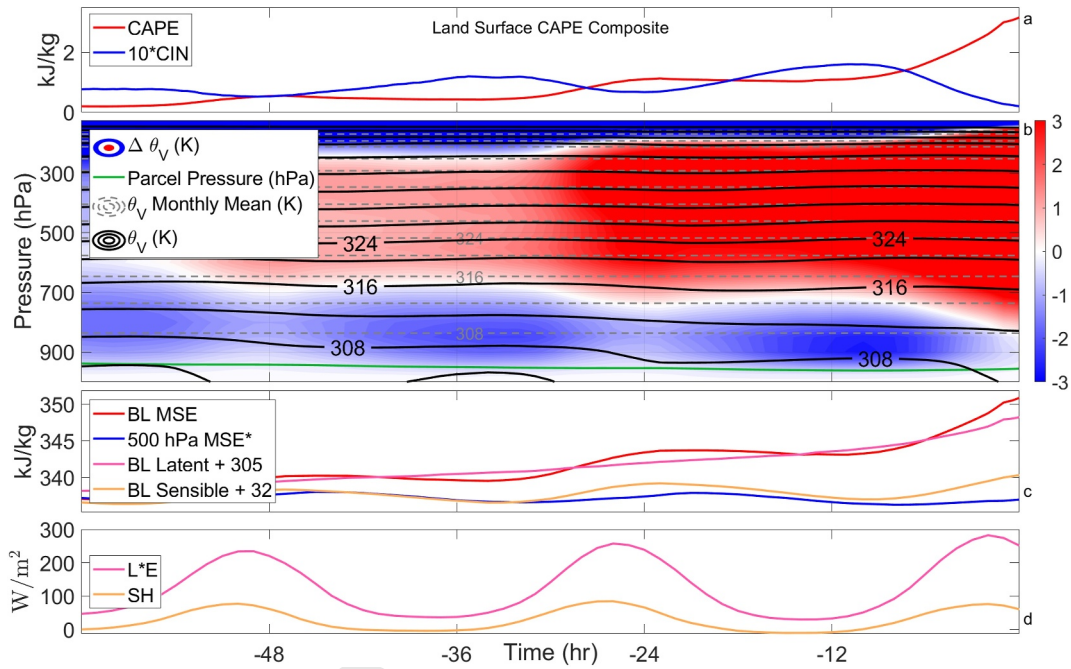

Figure 9. A composite of 256 "land surface CAPE" maxima. The quantities shown are the same as in Figure 4 but averaged across many maxima at a given time before that maximum. The monthly mean θ_V is averaged across that of each maximum.

different. Specifically, the seen θ_V contours rise dramatically in the 24 hr leading up to the time of maximum CAPE, indicating free troposphere cooling. CAPE can be thought of as a difference between a boundary layer MSE and free troposphere MSE* and in the other cases CAPE built up from an increase in boundary layer MSE, whereas in this case it grows due to a decrease in free troposphere MSE*. This is shown more explicitly in Figure 8c; the boundary layer MSE does not change significantly in the lead-up to the event, whereas the 500 hPa MSE* decreases significantly. As the free troposphere is controlling this CAPE buildup, other quantities, such as the CIN layer and surface fluxes, are not as relevant as they were in the previous cases. Due to the importance of free troposphere cooling for the buildup of an energy difference, we refer to this type of CAPE as "Troposphere Cooling CAPE," and similar occurrences are shown as red dots in Figure 2.

3.2. Composites

In this section, we study composites for each of the three types of high CAPE occurrences discussed above. To calculate these composites, we separate the studied CAPE maxima (Figure 2) into categories by defining an advection factor and surface flux factor. The advection factor is defined as the proportion of PCAPE increase over the 24 hr before the time of maximum CAPE that is due to a decrease in 500 hPa MSE*, and any occurrence with an advection factor greater than 1/3 is labeled a troposphere cooling CAPE maximum. The surface flux factor, defined as the maximum surface flux divided by the maximum + minimum surface flux over the final diurnal cycle, is used to separate the remaining events into land surface CAPE (surface flux factor>0.85) and land-sea CAPE. These factors are also used to color the dots in Figure 2, with the amount of red indicating the advection factor and the blue-green axis representing the surface flux factor.

A composite of land surface CAPE occurrences, that is, those with a large increase in boundary layer MSE and a strong diurnal cycle of surface fluxes, is shown in Figure 9. These events have a small CAPE increase the day before the day of maximum CAPE, but most CAPE buildup occurs on that day (Figure 8a). The CIN broadly increases from 2 days before the event up until a few hours before the event, when strong diurnal sensible heating decreases it to almost zero at the time of maximum CAPE. The CAPE accumulation is due almost entirely to changes in the boundary layer, as the free troposphere (<700 hPa) does not cool significantly over the 60 hr before these events (Figure 8b). The CIN buildup, on the other hand, has a significant contribution from the warming of the region between 950 and 750 hPa, which ends up several degrees warmer than the monthly mean at the same location. This implies that anomalously warm air needs to be advected over the boundary layer parcels in order to

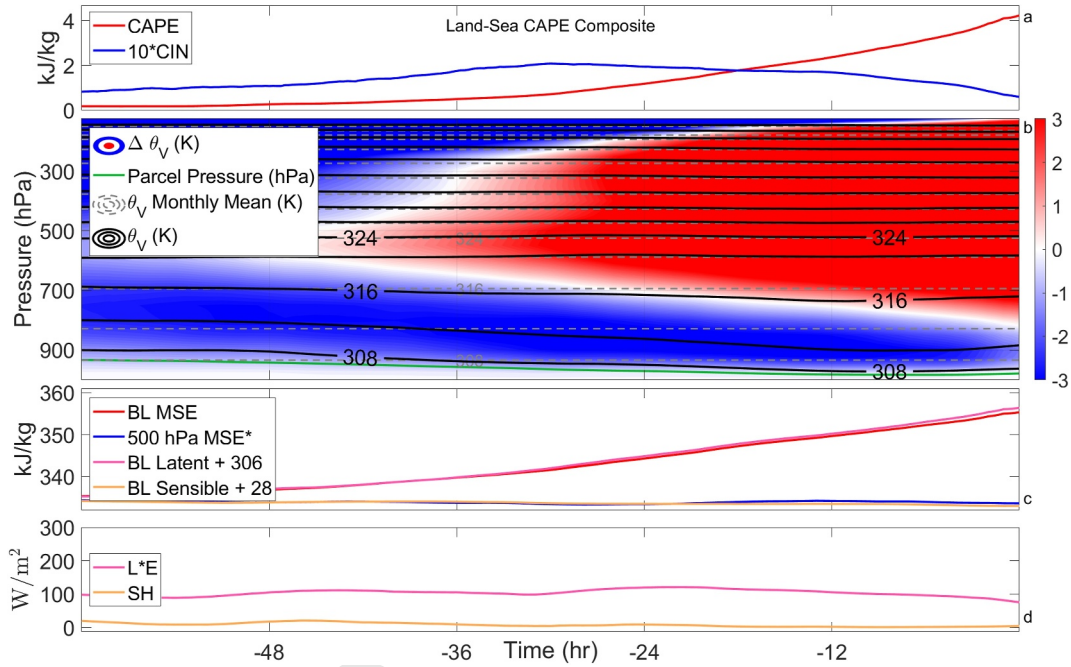

Figure 10. Same as Figure 9, composited across 152 "land-sea CAPE" maxima.

create a CIN layer that allows the CAPE to build up. Note that the temperature in this layer changes on the timescale of several days, whereas the diurnal cycle of CIN is mostly controlled by near-surface properties. Meanwhile, boundary layer MSE is increasing due to the accumulation of latent energy (Figure 8c) and has a diurnal cycle due to the sensible component of MSE. The seen MSE* does not change significantly over this time, though it has a small diurnal cycle (Figure 8c). As these events are occurring over land (by design), the surface fluxes have a large diurnal cycle (Figure 8d). Importantly, the daytime sensible heating on the day of maximum CAPE causes CIN to almost entirely vanish.

To summarize, CAPE builds up in "land surface CAPE" occurrences because anomalously warm CIN layer air traps boundary layer air for one or 2 days, allowing moisture to accumulate in the boundary layer, which increases CAPE. Then, the diurnal cycle of sensible energy erodes CIN, possibly initiating convection.

The situation is quite different for land-sea CAPE occurrences, a composite for which is shown in Figure 10. Rather than having diurnal cycles, CAPE builds up smoothly over the 36 hr before the time of maximum CAPE, and CIN decreases over most of this time. Once again, the free troposphere does not play a significant role in the CAPE buildup, as the contours above 700 hPa are flat (Figure 10b), and the seen MSE* does not change while CAPE is increasing (Figure 10c). Although there is some warming of the layer between 900 and 700 hPa before land-sea CAPE maxima, it is a much smaller effect than in the case of land surface CAPE maxima. For example, although the 308 K contour does drop slowly over the days before the event, it is always within a few degrees of climatology. The 312 K contour also moves down, but the difference from climatology is significantly smaller than in the previous composite. Instead, the relevant boundary layer parcels seem to be trapped under warm air for several days, implying that it is not so unusual for there to be CIN in these regions. The CAPE eventually builds up due to a large increase in latent energy in the boundary layer (Figure 10c, pink line), which is occurring day and night. There is almost no change in sensible energy, indicating that CIN eventually decreases due to the lifted condensation level lowering not the potential temperature of the boundary layer increasing. This can also be seen from the bottom of the red region moving down in Figure 10b. These changes in boundary layer energy match the surface fluxes, where evaporation is large and constant and sensible heating is negligible. This is to be expected for parcels over water, as oceans and seas have too large a heat capacity for there to be a significant diurnal cycle.

Land-sea CAPE maxima occur when boundary layer air receives moisture from the surface while trapped under a warm CIN layer, presumably from nearby land. These CIN layers are warmer than the monthly mean for the area

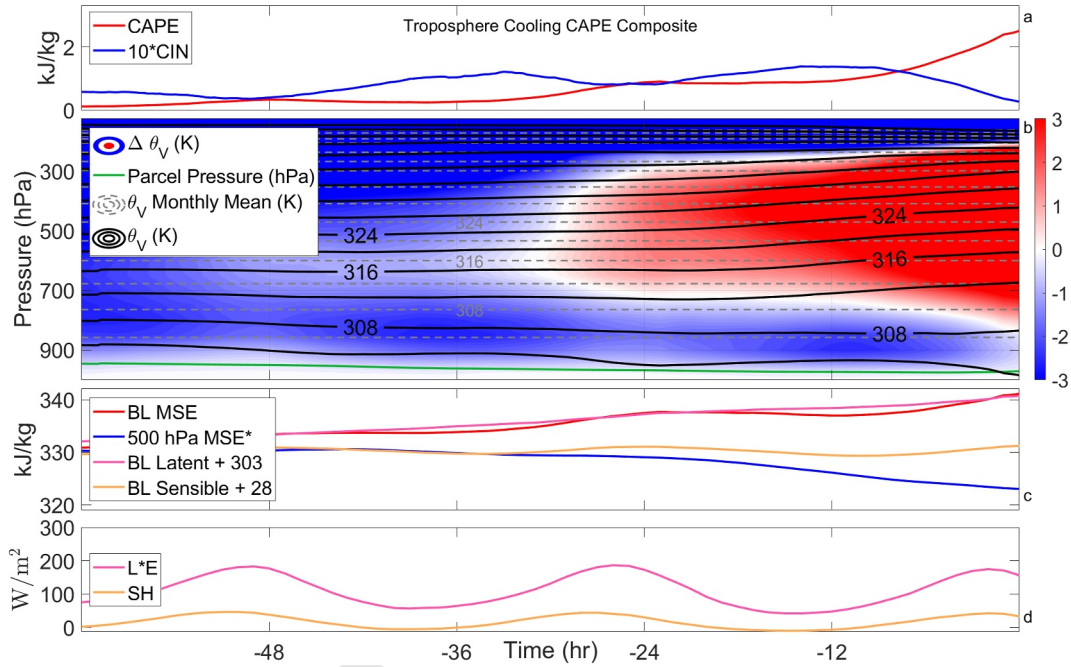

Figure 11. Same as Figure 9, composited across 211 "troposphere cooling CAPE" maxima.

but not by very much. In other words, there is often CIN in these regions, and it is merely the large buildup of water vapor in the boundary layer that leads to anomalously high CAPE.

Our final type of CAPE maximum, shown in Figure 11, is troposphere cooling CAPE in which a significant proportion (>1/3) of the PCAPE increase is due to a decrease in free troposphere MSE*. In these events, CAPE increases over the 2 days before the time of maximum CAPE with most of the increase happening on the day of the maximum (Figure 11a). Both the CAPE and CIN have diurnal cycles with the night before the CAPE maximum having the most CIN. Although the relevant example shown occurred over water, and therefore had a small diurnal cycle, about a quarter of troposphere cooling CAPE occurrences found were over land (surface flux factor <0.85), and it is these peaks that contribute to the diurnal cycle in the composite. The structure of changes in the θ_V profiles (Figure 11b) is quite different from those that lead to the other categories of CAPE maxima. Specifically, the θ_V contours in the free troposphere (<700 hPa) tilt upwards over the 14 hr before the time of maximum CAPE with a total change of a several degrees. The θ_V begins warmer than the monthly mean but ends up colder, indicating that it is anomalously cold air for the area causing this energy difference. The change in free troposphere energy can also be seen in the composite of 500 hPa MSE* (blue line, Figure 11c), which in this composite decreases significantly. The boundary layer MSE also plays a large role in the CAPE energy buildup, increasing by about 10 (kJ/kg). This is mostly due to the fact that events are included in this composite if at least 1/3 of the PCAPE increase came from troposphere cooling. Some events will have even more of the energy difference coming from cooling of the troposphere as with the sample event shown in Figures 7 and 8, and some will be closer to land surface events. As previously, the buildup of boundary layer MSE is mostly due to an increase in latent energy, whereas the sensible energy contributes a diurnal cycle.

To summarize, troposphere cooling events occur because there is anomalously cool air in the free troposphere above boundary layer parcels whose MSE may or may not be increasing. This is quite different from the other CAPE types in which the free troposphere does not play a significant role in the buildup of CAPE.

3.3. Regional Statistics

Having identified relevant characteristics of CAPE buildup, we wish to understand the distribution of the relevant statistics in each region (Figure 12). First, we show the distribution of CAPE values across the CAPE maxima in each region in the left panel with the regions sorted by the median CAPE value. The highest CAPE values worldwide are nearly all over the Persian Gulf or the Red Sea with the 25th percentile event there (~4.5 kJ/kg)

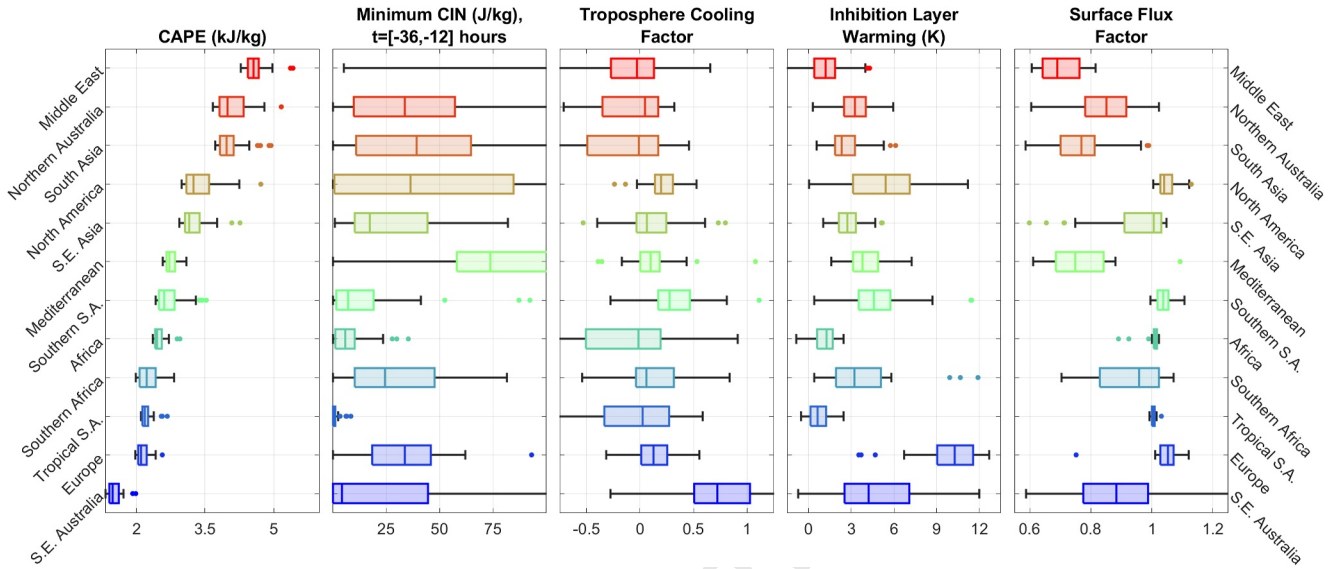

Figure 12. Statistics across CAPE maxima in each region for several relevant quantities: maximum CAPE (left panel), the minimum CIN the day before the day of maximum CAPE (second panel), the troposphere cooling factor (third panel), the CIN layer warming (fourth panel), and the surface flux factor (fifth panel). Each panel shows a box chart for each region, displaying the median (center line), the interquartile range (outlined box), and the minimum and maximum values (error bars) excluding outliers (defined as more than 1.5 times the interquartile range away from the box). Roughly 50 CAPE maxima are used in most regions, whereas 25 are used in South Africa, Europe, and the Mediterranean. The median value of minimum CIN in the Middle East is 203 J/kg, this is not shown so that smaller values can be distinguished, and any large values represent sufficient inhibition to prevent convection.

having more CAPE than the 75th percentile in any other region. The other regions which have a significant number of maxima around 4 (kJ/kg) are northern Australia and South Asia, whose CAPE maxima are almost exclusively on the sea side of a land-sea boundary. The regions which have the largest CAPE maxima over land, such as North America and Southeast Asia, most often have CAPE values around 3.5 (kJ/kg). Other regions have maximum CAPE values just over 2 (kJ/kg), whereas southeast (SE) Australia has maxima of less than 2 (kJ/kg).

Our next statistic of interest is one not discussed previously. All of the sample events and composites indicated CAPE building up over several days with at least some CIN preventing convection on the day before the time of maximum CAPE. However, it is not necessarily the case that CAPE builds up over several days in every case. Therefore, in the second panel of Figure 12, we display the minimum CIN between 12 and 36 hr before the time of maximum CAPE. If this value is large enough to prevent convection, then the tracked parcel will have been trapped during the previous diurnal cycle, so CAPE is likely to have built up over several days. However, if this value is small, then CAPE most likely built up entirely on the day of the maximum. In most regions, including the Middle East, northern Australia, South Asia, North America, the Mediterranean, southern Africa, and Europe, more than half of events have significant ($\geq$50 J/kg) CIN, indicating that the most convectively unstable profiles exist when CAPE is allowed to build up over more than 1 day. Note that this choice of 50 (J/kg) is arbitrary, as the amount of CIN which is needed to prevent convection will depend on several factors. In some other regions, including Southeast Asia, southern South America, and southeast Australia, there are fewer, but still several, events in which CAPE builds up over more than one diurnal cycle. Lastly, in tropical South America and Africa, nearly all events have no CIN the day before the time of peak CAPE, so the largest CAPE occurrences in those regions do not require the presence of a CIN layer over several days. This does not mean there was no CIN layer, as the night before the time of peak CAPE will likely have CIN even if the day before did not.

Our third statistic of interest is the troposphere cooling factor, that is, what proportion of the increase in PCAPE over the 24 hr before the time of maximum CAPE is due to free troposphere cooling. A value of one indicates that the boundary layer MSE has not changed, whereas a value of zero indicates that the 500 hPa MSE* has not changed. Most regions have medians around zero, indicating that CAPE builds up due to an increase in boundary layer MSE not the cooling of the free troposphere. However, there are a few regions whose distributions are to the right of the others: North America, southern South America, and southeast Australia. In North America, the distribution of the troposphere cooling factor has less variance than in other regions, and some events have a

roughly zero troposphere cooling factor but many have a troposphere cooling factor between 1/4 and 1/2. In southern South America, some occurrences have a factor of around a half but most have smaller values. In southeast Australia nearly all high CAPE events are due to troposphere cooling with a median troposphere cooling factor of almost 3/4. Overall, CAPE buildup is caused by boundary layer MSE increases in most of the world, but free troposphere cooling plays a small role in North America, a significant role in southern South America and a dominant role in the ocean regions off of Southeast Australia. There are also a few events scattered throughout other regions in which troposphere cooling plays a role (red dots in Figure 2), but these are rare.

As increases in boundary layer MSE are vital in causing CAPE buildup, a CIN layer is required to prevent convection while the MSE is increasing. Therefore, we use "inhibition layer warming" to understand the origin of the CIN layer, and it is defined as the seen θ_V at the pressure of maximum negative buoyancy and time of maximum PCIN subtracted from the monthly mean θ_V for that location, pressure, and time of day. In other words, if an event has far more CIN than usual for that area, it will have a large inhibition layer warming value, whereas if there is always a CIN layer in a certain area, we would expect little or no inhibition layer warming.

The regional statistics of inhibition layer warming are shown in the fourth panel of Figure 12. Tuckman et al. (2023) showed that CAPE maxima over North America are usually preceded by the presence of a CIN layer, which is anomalously warm for the area, and our results agree, showing that CAPE builds up in North America under an inhibition layer which, in the median, is 5 K warmer than the monthly mean. This is similar to the regional distribution in southern South America and less extreme than in Europe, where the median high CAPE occurrence is preceded by 10 K of inhibition layer warming. In other regions, however, CAPE is accompanied by less inhibition layer warming. Northern Australia, South Asia, Southeast Asia, the Mediterranean, and South Africa all have distributions centered between 2 and 5 K, whereas the Middle East, Africa, and tropical South America all have distributions indicating that very little inhibition layer warming is necessary for the buildup of CAPE. In Africa and the Middle East, the buildup of CAPE does not require an anomalously warm CIN layer, but extra moisture accumulation underneath a consistently warm CIN layer, probably originating over the Sahara. In tropical South America, however, the lack of inhibition layer warming is likely due to the fact that CAPE there tends to build up over only 1 day. Southeast Australia has a very wide distribution for inhibition layer warming, but this is not meaningful as most of the CAPE arises from free troposphere cooling.

Our final statistic used to characterize CAPE maxima, the surface flux factor, distinguishes land-sea CAPE maxima from land surface maxima (fifth panel of Figure 12). This factor is defined as the maximum total surface flux over the 24 hr before the time of maximum CAPE divided by the maximum plus minimum surface flux over the same period. If the surface fluxes reach zero at any point over the diurnal cycle, this factor will be 1, whereas if the surface flux is constant, it will be 1/2. Values close to 1 indicate that the boundary layer parcels are over land, whereas values closer to 1/2 indicate that the boundary layer parcels are over water. The CAPE peaks in each region mostly fall into one of these categories with events over Africa, eastern Asia, Europe, and the Americas having high surface flux factors and events in the Middle East and South Asia having low surface flux factors (see also Figure 2). In northern Australia, most events seem to have surface flux factors indicating ocean (<0.9), but a significant number are around one. In southeast Australia, there is an extremely wide distribution with some events having boundary layer parcels, which came from land and some from the surrounding ocean. It makes sense that the boundary layer parcel behavior would be less consistent in southeast Australia, as it is troposphere cooling that controls when these events occur rather than boundary layer warming. This statistic is especially relevant to convective initiation, as a small surface flux factor likely indicates that there will not be enough daytime sensible heating to overcome CIN after moisture builds up in the boundary layer. This can be seen as the leftover CIN at the time of maximum CAPE in the land-sea composite (Figure 10).

It is worth noting that the regional differences in inhibition layer warming do not line up particularly well with the differences in surface flux factors despite land-sea CAPE generally having less inhibition layer warming than land surface CAPE. For example, both the Middle East and northern Africa tend to have very little inhibition layer warming with a median of less than 1.5 K, but these regions have very different surface flux factors. The lack of inhibition layer warming is simply due to the proximity to the Sahara or Arabian deserts, whereas the Middle East tends to have maxima over water and Africa tends to have maxima over land. We chose to divide CAPE maxima into land surface CAPE and land-sea CAPE based on the surface flux factor as it has more of a bimodal distribution and is important for convective initiation, but one could also define a type of CAPE maximum with large

inhibition layer warming and one with little inhibition layer warming. To understand how CAPE tends to build up in a region, it is vital to understand both the diurnal cycle of surface fluxes and the origin of the CIN layer.

4. Conclusion

Severe convective events are usually associated with the release of CAPE. Therefore, studying how and why CAPE accumulates helps us understand the climatology and variability of severe convective events. We use three principal factors to characterize the origin of high CAPE at a given time: (a) a troposphere cooling factor, (b) an inhibition layer warming factor, and (c) a surface flux factor. The troposphere cooling factor represents the extent to which CAPE builds up due to cooling aloft rather than to increases in boundary layer moist static energy, and we find that only in southeast Australia is CAPE buildup dominated by troposphere cooling. Many CAPE maxima in North America and southern South America have some contribution from troposphere cooling, and elsewhere CAPE buildup is entirely controlled by increases in boundary layer MSE.

As CAPE buildup tends to be due to boundary layer warming or moistening, CIN is required to prevent convection while energy is accumulating in the boundary layer. Our second quantity used to characterize CAPE maxima is therefore the inhibition layer warming, indicating whether a CIN layer requires anomalously warm air for that area or if that layer is always warm. We find that near the Sahara or the Arabian Peninsula (i.e., in central Africa and the Middle East), the inhibition layer does not need to be significantly warmer than usual to allow for the buildup of CAPE. In most regions around the world, inhibition layer warming of 2–5 K can allow for the buildup of CAPE, whereas in North America and Europe, significantly more inhibition layer warming (5–10 K) occurs before a high CAPE occurrence. Some regions, such as tropical South America, have CAPE maxima in which the energy buildup occurs over only one diurnal cycle, therefore not requiring the presence of a CIN layer on the previous day.

Our last identifying characteristic, the surface flux factor, is a measure of the diurnal cycle in surface fluxes over the day before a CAPE maximum. This diurnal cycle is important for convection as a lack of daytime sensible heating can prevent boundary layer air from overcoming the CIN layer and therefore prevent the initiation of deep convection. High CAPE occurrences over land, such as those in the Americas, Africa, and Europe, tend to have large values of surface flux factors and therefore may have enough sensible heating for CIN to become very small. However, high CAPE occurrences in other regions tend to be over the ocean or seas and are unlikely to receive enough sensible heat from the surface to trigger deep convection.

These results have significant implications for the study of CAPE and therefore severe convective events. First, they show that if we wish to understand convective events, we must consider the local environment, as CAPE builds up in different ways in different regions. This is also true if we want to understand how CAPE will change under global warming or given a shift in land types; we must consider each region separately. The study of how climate change will affect severe convective events is underway (Botzen et al., 2010; Del Genio et al., 2007; Dessens, 1995; Kunkel et al., 2013; Seeley & Romps, 2015; Trapp & Hoogewind, 2016; Trapp et al., 2007) and often focuses on specific regions (Chen et al., 2020; Gensini & Mote, 2015; Hoogewind et al., 2017; Púčik et al., 2017), but work on how CAPE buildup will change with warming may provide useful insights.

Second, our results emphasize the importance of surface properties for the buildup of CAPE. In most of the world, boundary layer energy buildup is the principal cause of CAPE, and the changes in boundary layer energy match reasonably well with local surface fluxes. Therefore, in order for there to be CAPE buildup, there must be sufficiently high total surface fluxes to yield high enough low-level MSE, and there must be enough evaporation for boundary layer MSE and CAPE to build up before the sensible heating overcomes the CIN. Of critical importance in land surface CAPE cases is the partitioning between latent and sensible heating during diurnal surface heating. Emanuel (2023) showed that this partitioning as well as the total surface flux is highly sensitive to soil and vegetation properties.

This work has made progress toward understanding CAPE buildup and how it differs among various regions. However, we have not explained quantitatively why the Middle East, Northern Australia, and South Asia have larger CAPE maxima than the rest of the world, or why troposphere cooling CAPE maxima tend to be of smaller magnitude than others. Additionally, our results agree with previous work that suggests the importance of surface moisture gradients in the buildup of CAPE (Emanuel, 2023) but only qualitatively. Using the knowledge gained in this work, it may be possible to identify the fundamental drivers of the magnitude and frequency of CAPE maxima

by looking at local surface properties and near-surface wind in various regions (Li et al., 2024; Munday et al., 2023). This is an important step in quantitatively predicting and understanding CAPE maxima and therefore severe convective events.

Appendix A: Use of Reanalysis Data

ERA5 reanalysis data was a vital tool in conducting this research, as it allows Lagrangian tracking of parcels of air and estimation of air properties anywhere in the world. Although there is precedent for using ERA5 to analyze CAPE, it certainly has biases and errors, so in this appendix, we use a few case studies to compare ERA5 to observations. We explore differences between observed soundings and reanalysis, discuss implications for our results, and show why equatorial Africa was excluded from our analysis despite having severe convective events and high CAPE occurrences. This appendix is not a systematic study, but it gives a sense of how we expect reanalysis to compare to observations in various regions and what types of differences there will be.

We use sounding data retrieved from https://weather.uwyo.edu/upperair/sounding.html and compare them to the reanalysis data described in Section 2. In equatorial Africa, few soundings are available from this source, so we use soundings taken in Ouesso, Congo from https://data.ceda.ac.uk/badc/ukmo-rad/data/congo/ouesso. ERA5 reanalysis is run on a spectral grid of finite resolution, whereas observed soundings are taken at a specific point in space, so we would not expect perfect matches even if reanalysis data had no bias. Specifically, sounding data should be far more variable, while reanalysis should be smoother. In this appendix, we give eight examples of comparisons between reanalysis and sounding data from six different locations. We conclude that although there is certainly some error in reanalysis everywhere in the world; in most cases, these errors are rare or small enough that we believe our conclusions are valid. Over equatorial Africa, on the other hand, observations are rare and often differ enough from reanalysis data that our methods cannot be used to draw conclusions about high CAPE occurrences in that region.

Our first example is from the beginning of July 2012, near Minneapolis, Minnesota, United States (45°N, 93.25°W in reanalysis, MPX station for soundings) and is chosen due to its proximity to the first sample CAPE maximum displayed in Figure 3. At the time of each sounding from July 1 to 6, the $\Delta\theta_V$ of parcels lifted from 975, 950, 925, and 900 hPa are calculated throughout the relevant column for the soundings and reanalysis. The resulting CAPE and CIN are also computed, and these results are displayed in Figure A1 with the parcel lifted form 925 hPa represented by lines, and the error bars representing the range of values achieved from the other lifted parcels. Although these are not technically "uncertainties," the error bars indicate the range of possible values achieved, and we can understand these ranges as being due to variability in one data set that may or may not exist in the other.

In both reanalysis and soundings, there is a substantial amount of CAPE over the first 3 days of July 2012, a local minimum of CAPE at 6 a.m. local time on July 3rd, then another period of some CAPE over the next few days. However, the amount of CAPE is quantitatively different with consistently less CAPE in reanalysis than in soundings. Meanwhile, there is a small amount of CIN in both reanalysis and soundings throughout this period with slightly more CIN in reanalysis.

Although the values of CAPE are important, the vertical structure of buoyancy is of more direct relevance to the conclusions of this work. Therefore, we show $\Delta\theta_V$ at the time of each sounding in the bottom panels. The accuracy of reanalysis as well as the size of the error bars in the soundings varies significantly over this period. In most snapshots, reanalysis $\Delta\theta_V$ is within uncertainty at almost every vertical level, and it does especially well in the first, fourth, fifth, seventh, and eleventh time steps. However, reanalysis is sometimes significantly different from the sounding, such as on July 1 at 6 p.m. (3rd column); more detail about this time is shown in Figure A2. At that time, the temperature (left panel) is an extremely good match between reanalysis and soundings with very few discrepancies and none in the lower troposphere. However, the humidity (middle panel) is quite different in reanalysis and soundings, especially in the lower levels, where the sounding humidity is significantly larger. This has a large effect on $\Delta\theta_V$ (right column), as that humidity becomes excess buoyancy above the lifted condensation level.

By contrast, on July 2nd, at 6 p.m. (fifth panel, and Figure A3) the reanalysis and sounding $\Delta\theta_V$ are very similar. The range of sounding values due to lifting from different pressures is large, and we can look at the temperature (left panel) and humidity (central panel) to understand why. The temperature is once again a near perfect match

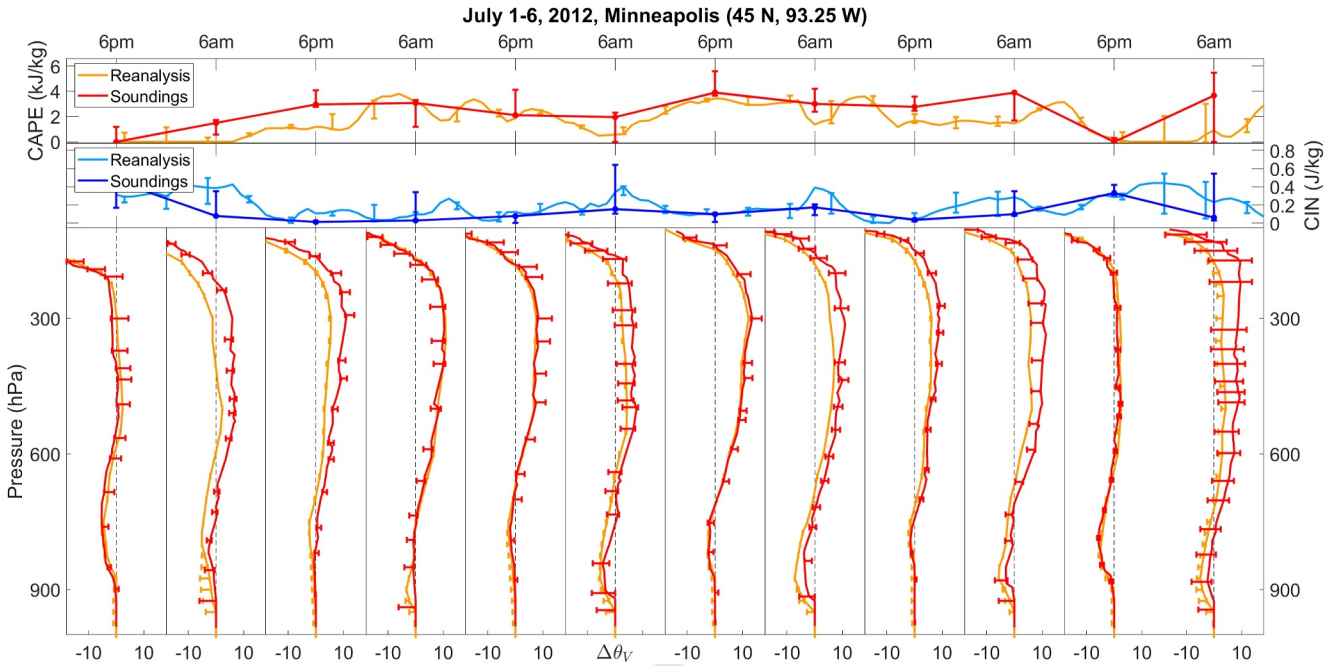

Figure A1. Comparing reanalysis (dashed) and sounding (solid) data for Minneapolis in the first 6 days of July 2012. Time series of CAPE (top panel) and CIN (middle panel) are shown as well as vertical profiles of $\Delta\theta_V$ (lower panels, parcel lifted from 925 hPa) every 12 hr from midnight GMT (∼6 p.m. local time) on July 1 to noon GMT on July 6 (∼6 a.m. local time). Vertical dashed lines indicate zero. The ticks indicate midnight/noon GMT, or 6 p.m./a.m. local time. Error bars indicate the range of results achieved by lifting from 975, 950, 925, and 900 hPa. Note that the first sounding is from 6 p.m. June 30, local time, as this corresponds to midnight, July 1, UTC.

between reanalysis and humidity with small differences in the middle troposphere. The sounding humidity, however, is much more variable in the lower troposphere. The low level humidity variability creates wide error bars in $\Delta\theta_V$ (right panel) for the sounding, as the buoyancy is very sensitive to the humidity of the lifted parcel.

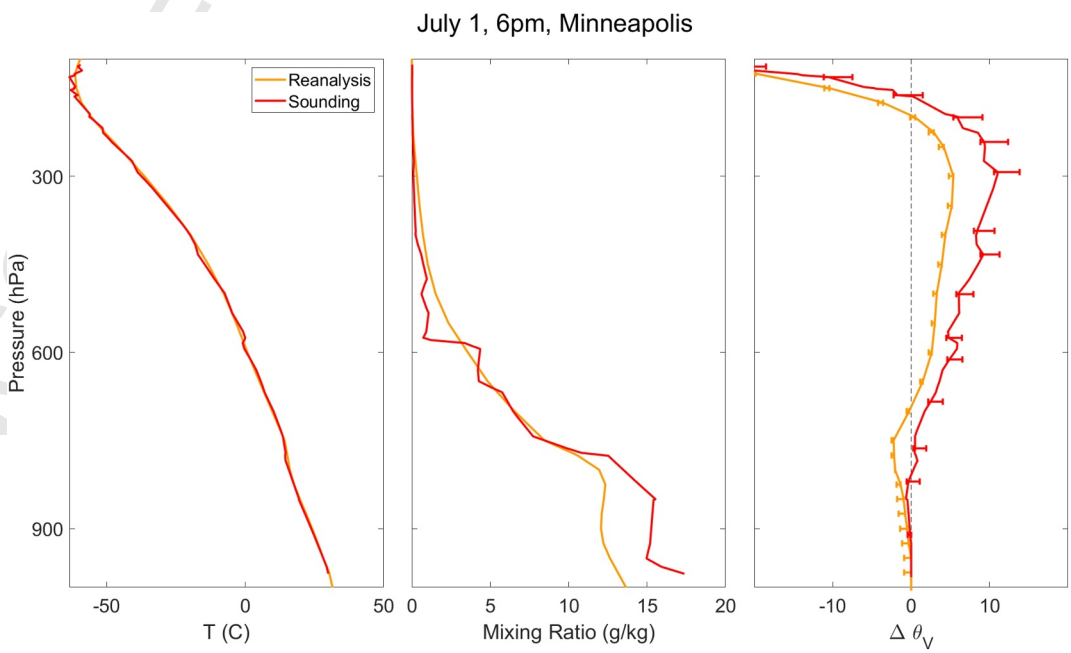

Figure A2. Temperature (left), mixing ratio (middle) and $\Delta\theta_V$ profiles for reanalysis (orange) and sounding (red) data from 1 July 2012, 6 p.m., near Minneapolis, USA. The error bars in the third panel correspond to the range of $\Delta\theta_V$ achieved from lifting the parcels at 975, 950, 925, and 900 hPa.

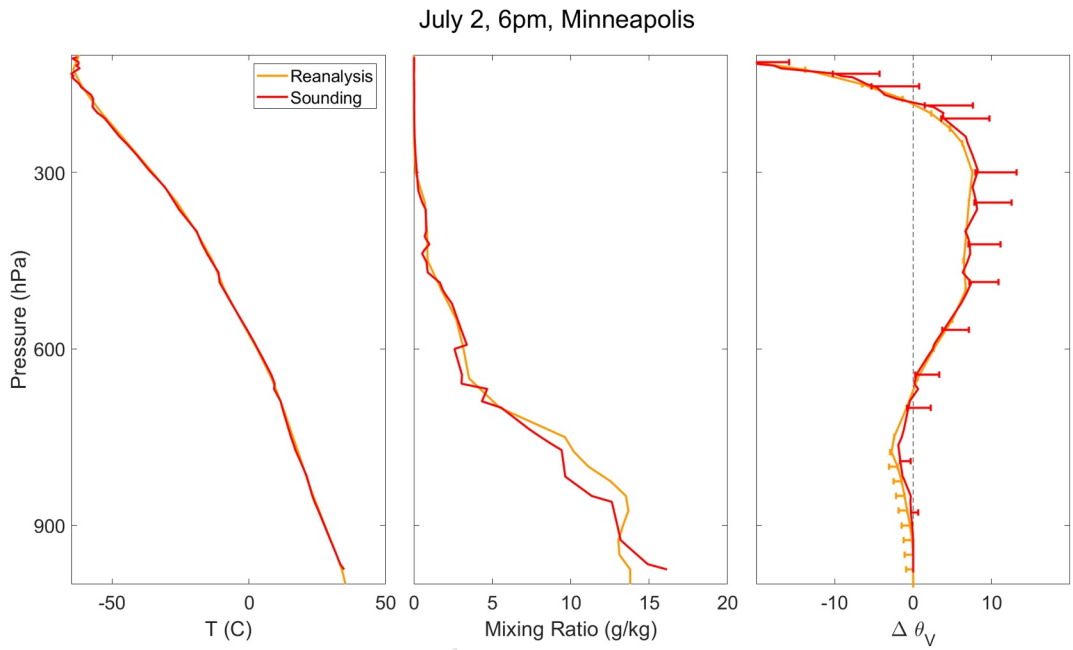

Figure A3. As for Figure A2 but for July 2, 6 p.m.

We show a third sample time in which the sounding has large error bars on $\Delta\theta_V$, but the "best estimate" from the soundings does not match reanalysis well. On July 3rd, 6 a.m. (6th snapshot in Figures A1 and A4), there is a substantial CAPE and CIN in both reanalysis and the sounding. The best estimate from the sounding has less CIN and more CAPE, but the uncertainty includes the values of reanalysis. This is because the near surface humidity of the sounding is extremely variable below 900 hPa. The exact choice of which of these parcels to lift will dramatically change the sounding $\Delta\theta_V$, but not that of reanalysis. As with the other soundings, the temperature matches well. At first glance, it would appear that this is an example of reanalysis having significant bias compared to the sounding, but it may simply be due to the nature of the reanalysis product.

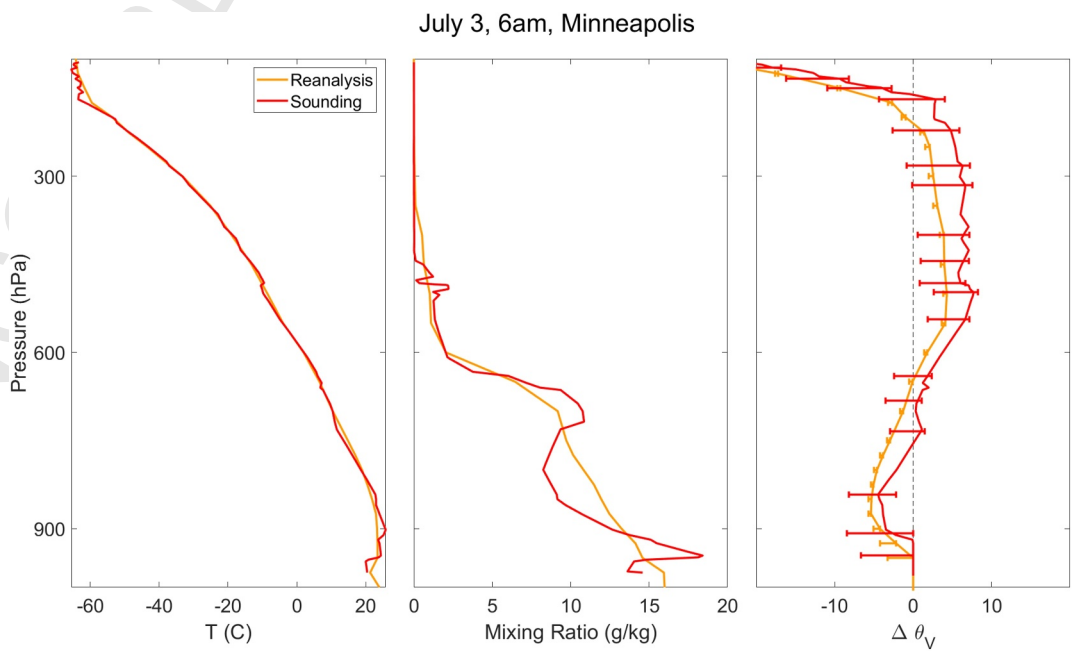

Figure A4. As for Figure A2 but for July 3, 6 a.m.

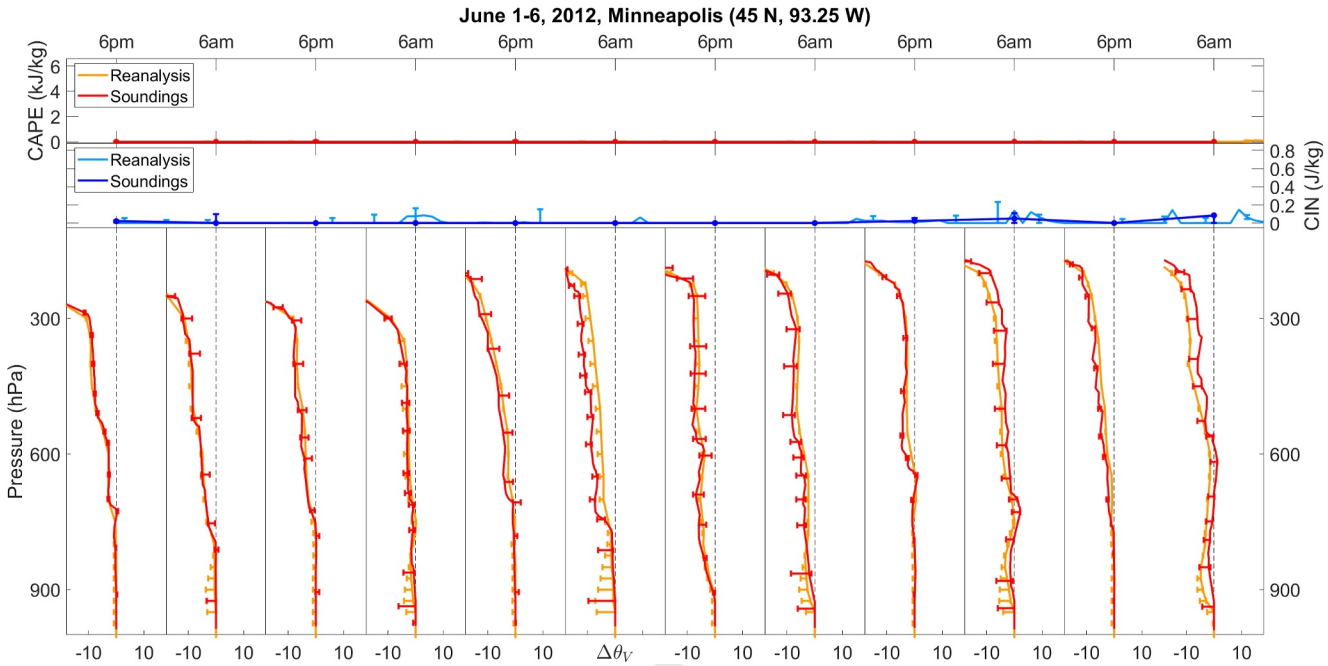

Figure A5. Same as Figure A1 but for June. The ticks indicate midnight/noon GMT or 6 p.m./am local time.

Next, we wish to look at soundings from Minneapolis at a time of low CAPE. Figure A5 shows the same quantities as Figure A1 but for June 2012. Both reanalysis and soundings show no CAPE and undefined/no CIN for these days. The vertical structure of $\Delta\theta_V$ matches very well between the two data sources in this case with the exception of June 3rd, 6 a.m.

At that time, there is significantly more negative buoyancy above 700 hPa in the sounding than in reanalysis. Figure A6 demonstrates that this is due to low level humidity being smaller in the reanalysis data than in the sounding.

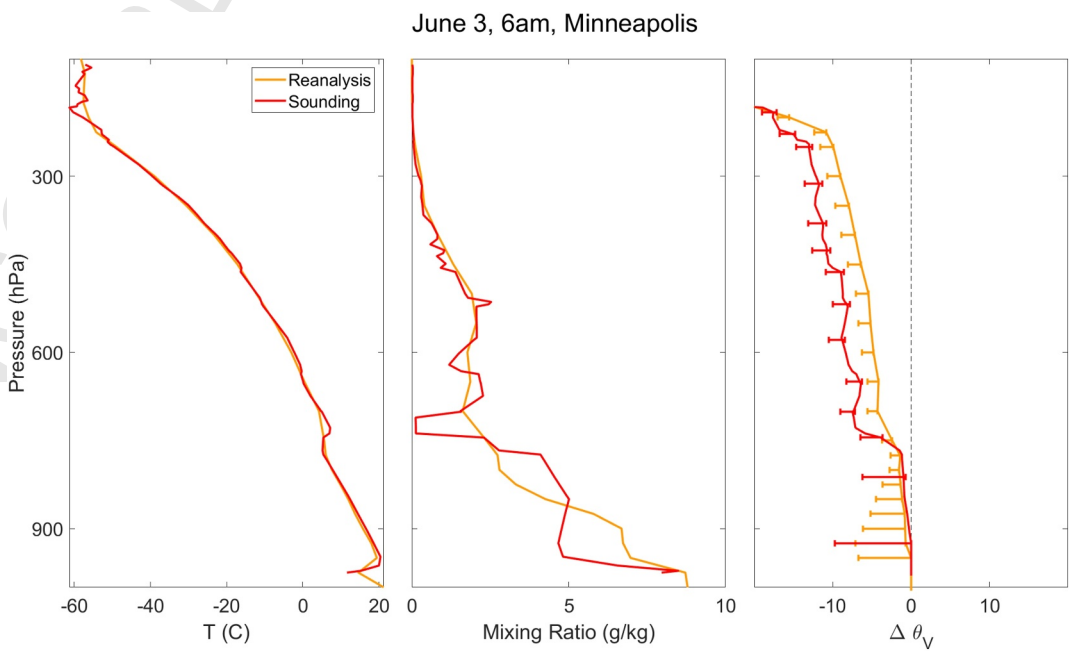

Figure A6. As for Figure A2 but for June 3, at 6 p.m.

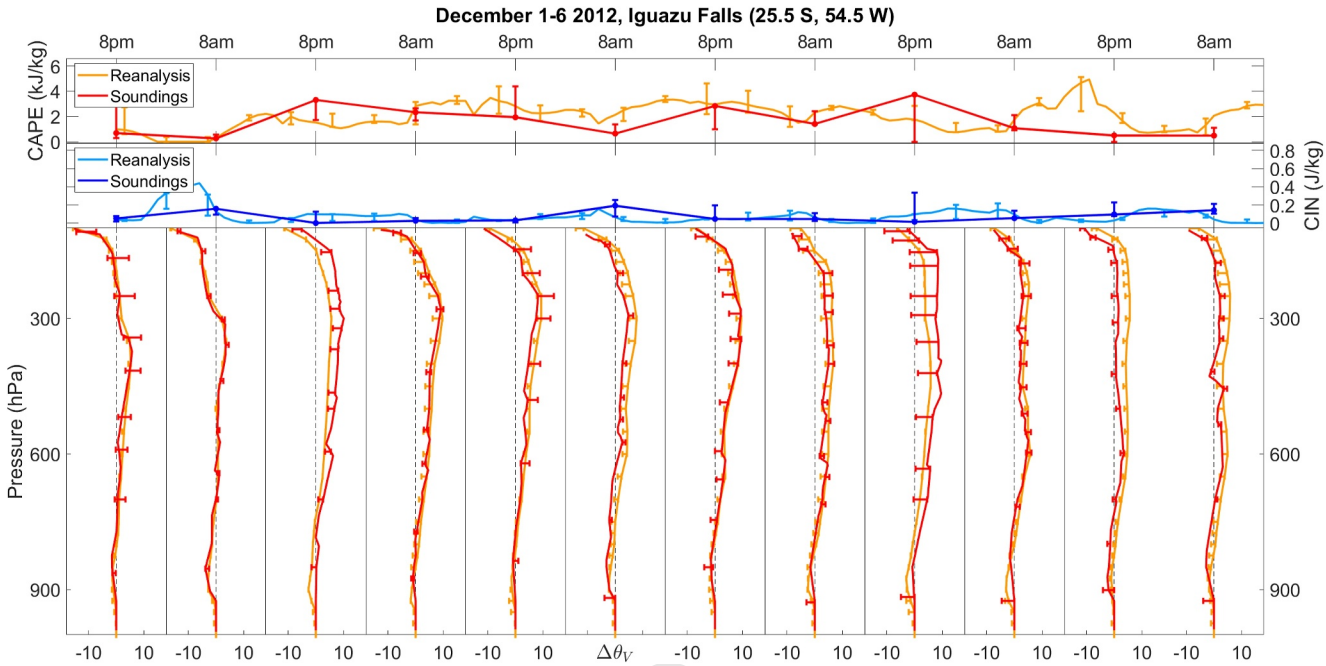

Figure A7. Same as Figure A1 but for Iguazu falls in the first 6 days of December 2012. The ticks indicate midnight/noon GMT or 8 p.m./a.m. local time.

Overall, we believe that the reanalysis does a reasonable, but not perfect, job of matching observations in Minneapolis, Minnesota, a region with relatively abundant observations. The nature of reanalysis, as a gridded product with finite resolution, implies that the data will be artificially smoothed, and this can dramatically change convective properties when applied to low level humidity. Additionally, there are several examples of reanalysis systematically underestimating or overestimating low level humidity, but we cannot determine from the data here whether this is also due to the averaging over a large area.

Our second sample location is Iguazu falls, Brazil (25.5°S, 54.5°W in reanalysis, the SBFI station for soundings), and we examine the first few days of December 2012 (Figure A7). Overall, the quality of the match between reanalysis and observations here is similar to in Minneapolis with reanalysis being within uncertainty of most soundings but having a few large discrepancies (on December 3 and December 5 at 8 p.m. local time). It is worth noting that at the two times where reanalysis does not match the sounding, the uncertainty in the soundings is large.

A snapshot at a time with large uncertainty is given in Figure A8 from December 3 at 8 p.m. As with the soundings over Minnesota, it is clear that the large uncertainty in the sounding $\Delta\theta_V$ is due to variations in lower level humidity. The differences between sounding and reanalysis at other times are, as before, due to biases in low level humidity (not shown).

Our third example location is Majuro, an equatorial Pacific island, chosen due to its representing an ocean climate. This is important as many of our high CAPE occurrences take place over water, but soundings tend to be over land. Figure A9 shows CAPE, CIN, and $\Delta\theta_V$ in soundings and reanalysis for the first 6 days of July 2012. Almost all of the $\Delta\theta_V$ profiles match well between reanalysis and observations with the exception of 4 July 2012, at 11 p.m. Additionally, the first two soundings have large uncertainties.

The large uncertainties in Majuro, just as in previous examples, are due to variable low level humidity (e.g., Figure A10). Interestingly, the sudden changes in humidity in this example may be due to observational error, as it is unlikely that humidity changes as quickly with height as is indicated by the observations.

The time in which Majuro profiles do not match between reanalysis and soundings is shown in Figure A11. This is the most extreme example so far of reanalysis not being reliable, as it systematically underestimates humidity and temperature everywhere below 650 hPa. This leads to a large difference in $\Delta\theta_V$ above this layer. Although this discrepancy is concerning, it is the exception, and most reanalysis data studied in Majuro is within uncertainty of

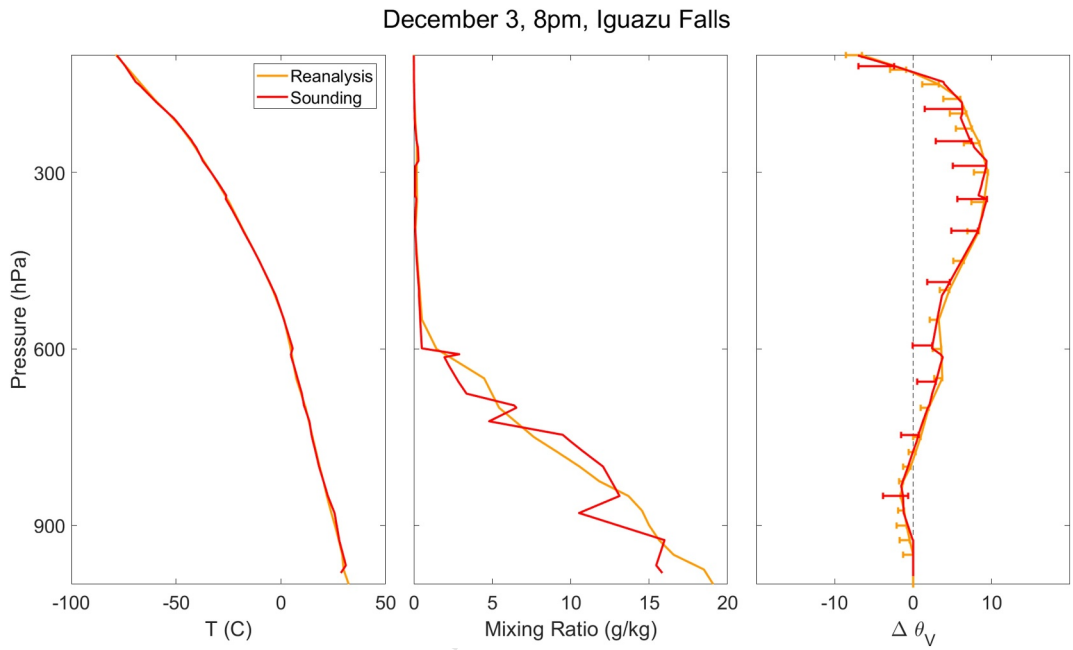

Figure A8. As for Figure A2 but for Iguazu Falls, Brazil, on 1 December 2012, at 8 a.m.

the soundings. It is also worth noting that the uncertainty in $\Delta\theta_V$ from this sounding includes zero (Xu & Emanuel, 1989).

Another ocean-like climate, that of Puerto Princesa in the Philippines, is explored in Figure A12. In this example, reanalysis overestimates $\Delta\theta_V$ almost half the time (first, fifth, sixth, eight, and tenth panels) and is roughly accurate the rest of the time. However, even when this overestimation occurs, reanalysis is often within uncertainty of the soundings. These examples (not shown) are similar to previous ones where reanalysis overestimates low level humidity, but the mixing ratio in the soundings is highly variable near the surface.

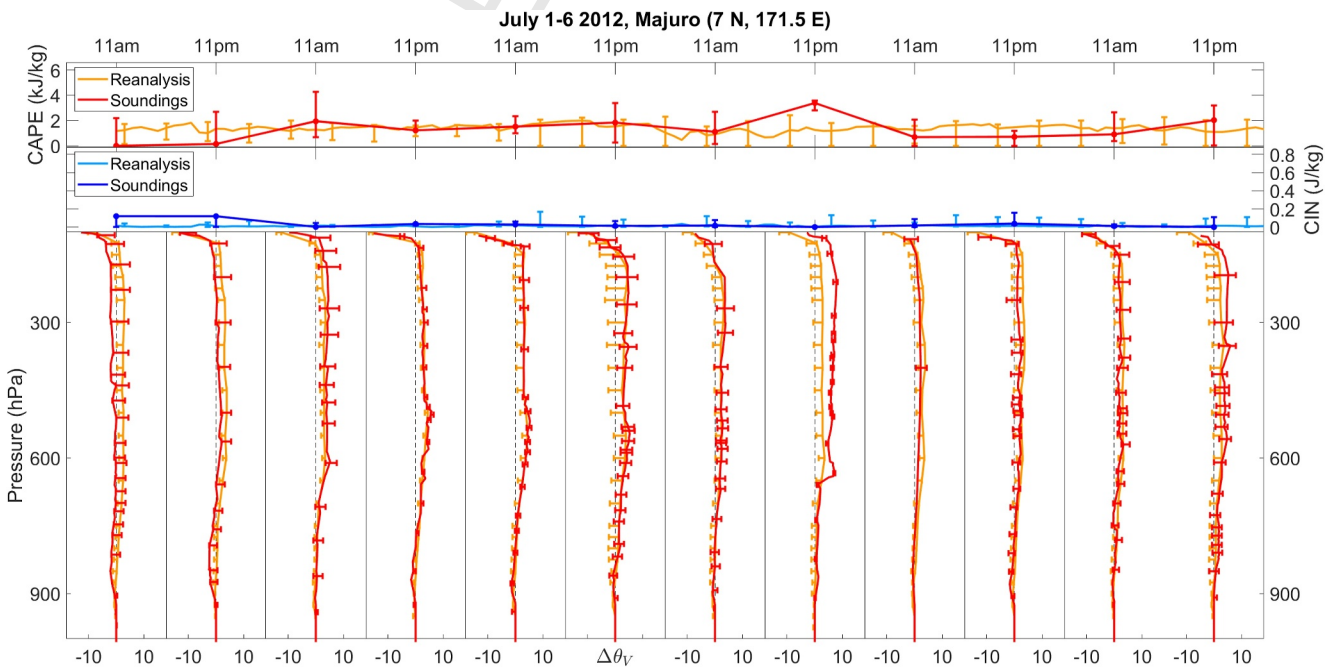

Figure A9. Same as Figure A1 but for Majuro in the first 6 days of July 2012. The ticks indicate midnight/noon GMT or 11 a.m./p.m. local time.

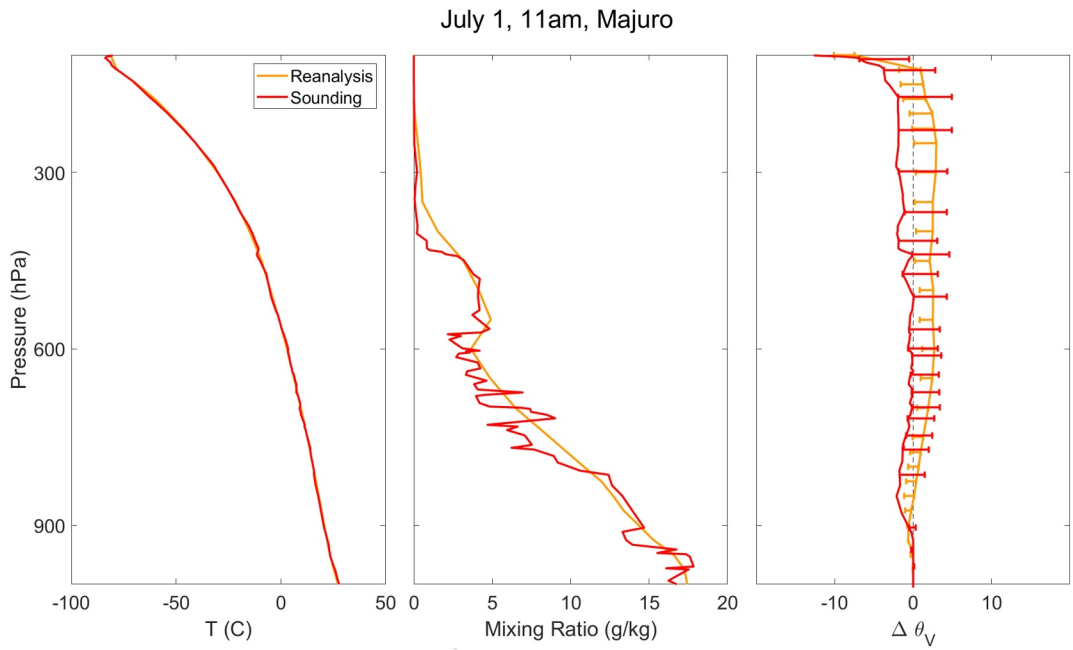

Figure A10. As for Figure A2 but for Majuro, Marshall Islands, on 1 July 2012, at 11 a.m.

In Iguazu falls and the two ocean climates studied, there are important and somewhat frequent errors in reanalysis. Despite this, on most days, the reanalysis $\Delta\theta_V$ profile is plausible given the nature of the product, and we believe that our conclusions will not be affected by the times when reanalysis systematically overestimates or underestimates the near-surface humidity in these regions.

Finally, we wish to assess reanalysis in a region where there are relatively few observations, that is, tropical Africa. We first study soundings from Ouesso, Congo and then from Ouagadougou, Burkina Faso. The soundings in equatorial Africa (Ouesso) are rare and differ significantly from reanalysis. However, soundings from just

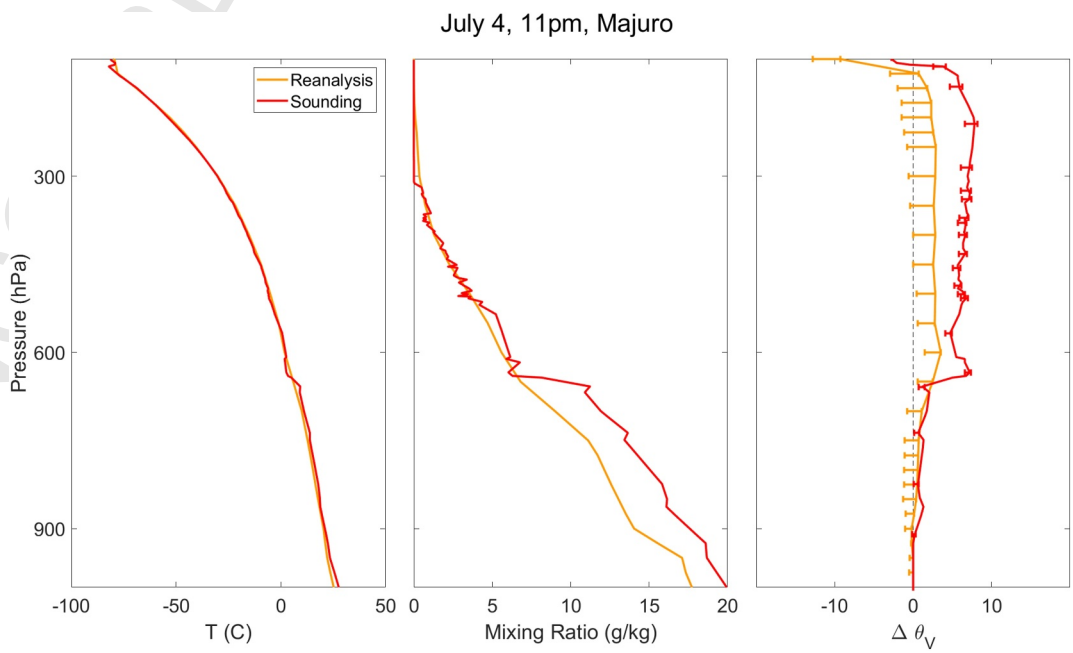

Figure A11. As for Figure A2 but for Majuro, Marshall Islands, on 1 July 2012, at 11 a.m.

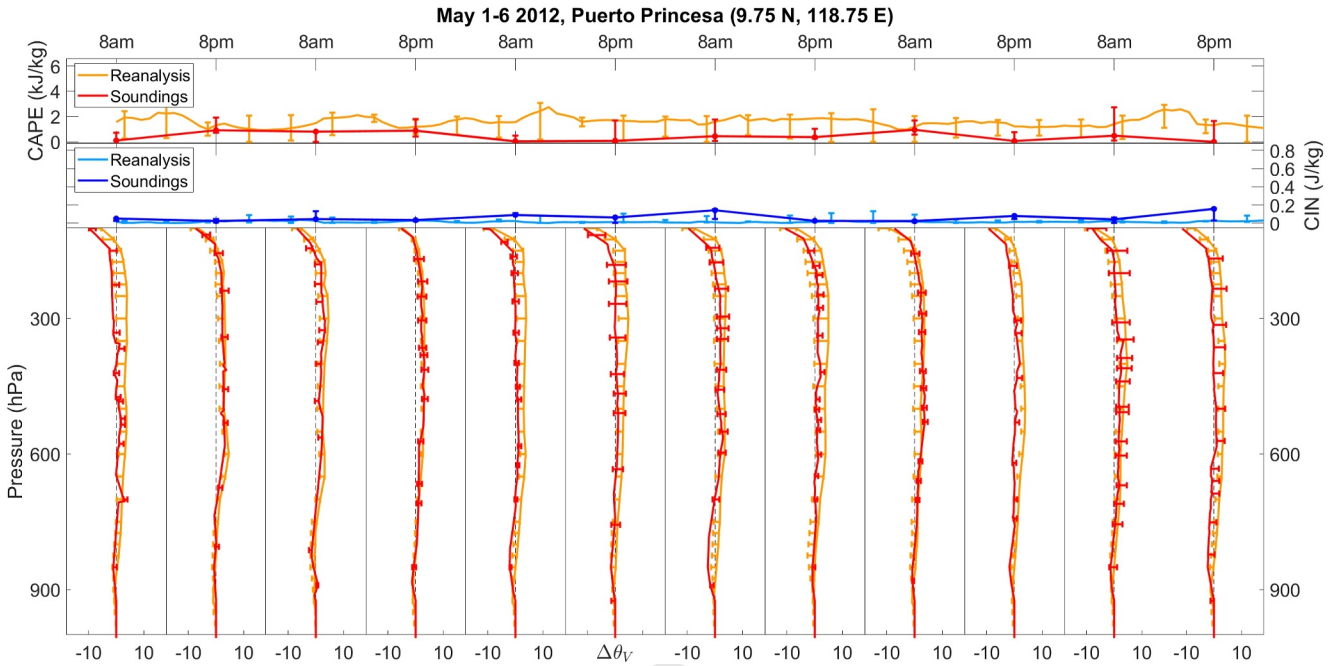

Figure A12. Same as Figure A1 but for Puerto Princesa in the first 6 days of May 2012. The ticks indicate midnight/noon GMT or 8 a.m./p.m. local time.

south of the Sahara (i.e., those from Ouagadougou) match reanalysis better. The sounding data from Ouesso were retrieved from https://data.ceda.ac.uk/badc/ukmo-rad/data/congo/ouesso.

We analyze two sets of soundings from Ouesso, first from 1 to 6 August 2013 and then from 1 to 6 December 2012. In the first time series (Figure A13), the reanalysis data consistently have more CAPE than the soundings with significant CAPE nearly every afternoon. Although CAPE does not match well, the vertical structure of $\Delta\theta_V$

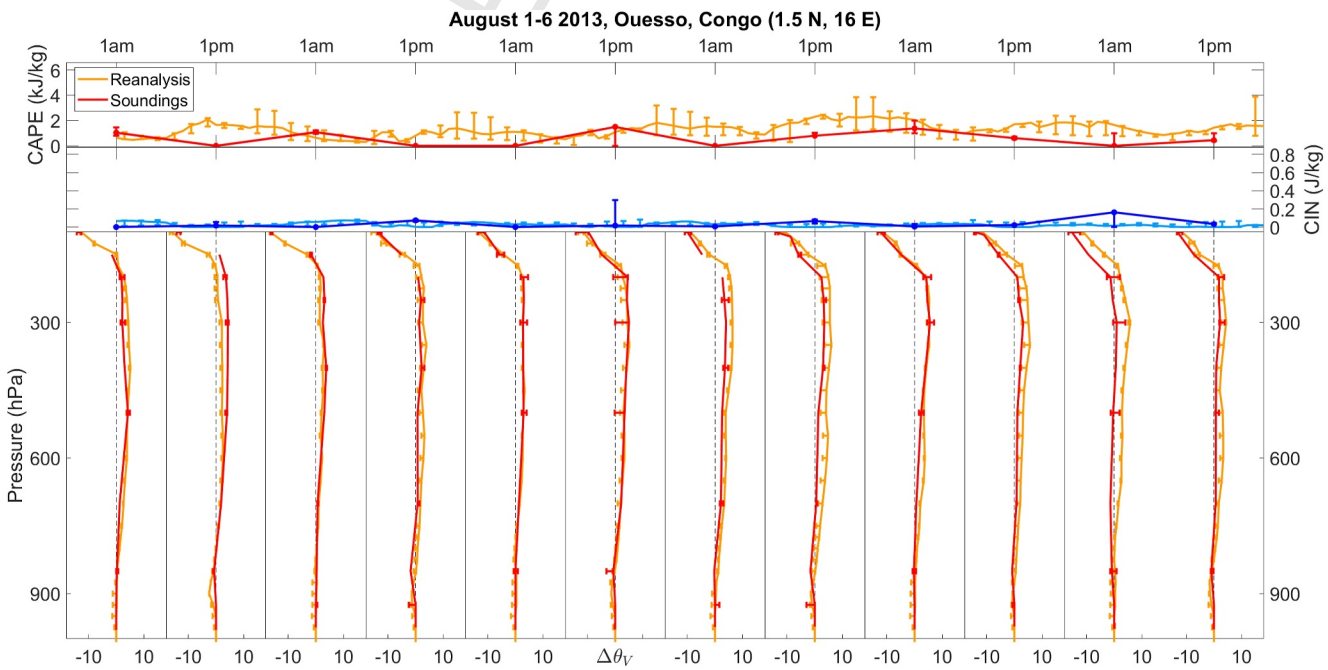

Figure A13. Same as Figure A1 but for Ouesso in the first 6 days of August 2012. The ticks indicate midnight/noon GMT or 1 a.m./p.m. local time.

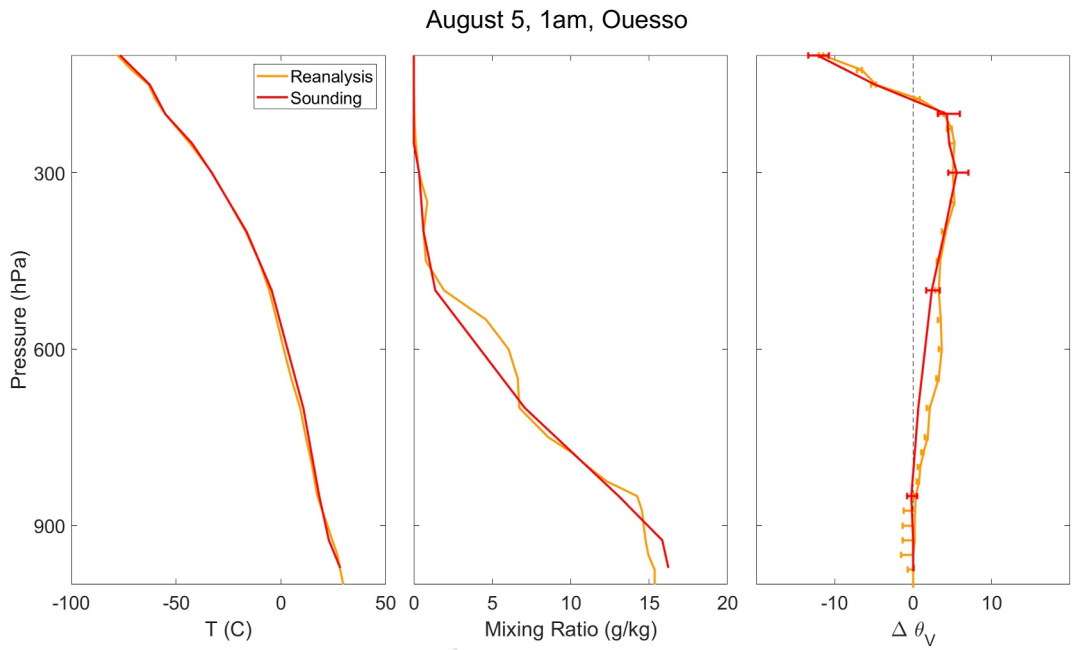

Figure A14. As for Figure A2 but for Ouesso, Congo, on 5 August 2012, at 1 a.m.

is much better. Specifically, although there are very few data points from the soundings, they tend to be within uncertainty of reanalysis with the largest exception of August 6, at 1 p.m.

Soundings that do not compare well between reanalysis and soundings in Ouesso will be discussed later, first we look in more detail at a well-represented sounding that of August 5, 1 a.m. (Figure A14). In this example, the humidity at low levels is slightly higher in soundings than in reanalysis, but the values are similar. However, the mid-troposphere temperature is slightly lower in reanalysis, leading to a more positive $\Delta\theta_V$ in that region. Unlike in previous examples, the vertical resolution of reanalysis is better than that of the sounding, so reanalysis can appear more variable.

Remaining in Ouesso, we now study soundings from December 2012 (Figure A15). Here, reanalysis is much worse at capturing the sounding structure than in all previous examples. The total amount of CAPE is significantly higher in reanalysis than in soundings at almost all times, and it is rarely within uncertainty.

For the $\Delta\theta_V$ profiles, reanalysis is not within uncertainty of the sounding for much of the free troposphere in about half of the soundings. The soundings are incomplete at some times, an example of which is shown in Figure A16. At this time, the sounding reached only about 400 hPa. Regardless, we see that reanalysis has excess humidity in the lower troposphere, leading to excess $\Delta\theta_V$ throughout the part of the column for which we have data. In this case, the sounding does not reach the level of neutral buoyancy, and so the total amount of CAPE is not meaningful.

Next, we show the reason for the anomalously large error bars in the 11th panel of Figure A13. In this example, the reported temperature and dew point temperature at 970 hPa are unreasonable (359 and 355 K, respectively, Figure A17). This leads to a large amount of $\Delta\theta_V$ when lifting from this level of the atmosphere, causing a huge uncertainty. Overall, soundings from Ouesso do not match reanalysis as well as those of the previous locations.

Our last set of soundings is from Ouagadougou, Burkina Faso, taken during the beginning of July 2012 (Figure A18). These soundings, retrieved from https://weather.uwyo.edu/upperair/sounding.html, are available only once every 24 hr and reach only around 300 hPa. The total sounding CAPE is not meaningful, as the height of the level of neutral buoyancy is unknown. Therefore, we focus on the vertical profile of $\Delta\theta_V$. Overall, reanalysis matches the soundings rather well except for a large difference on July 1 and a large uncertainty in the sounding on July 4.

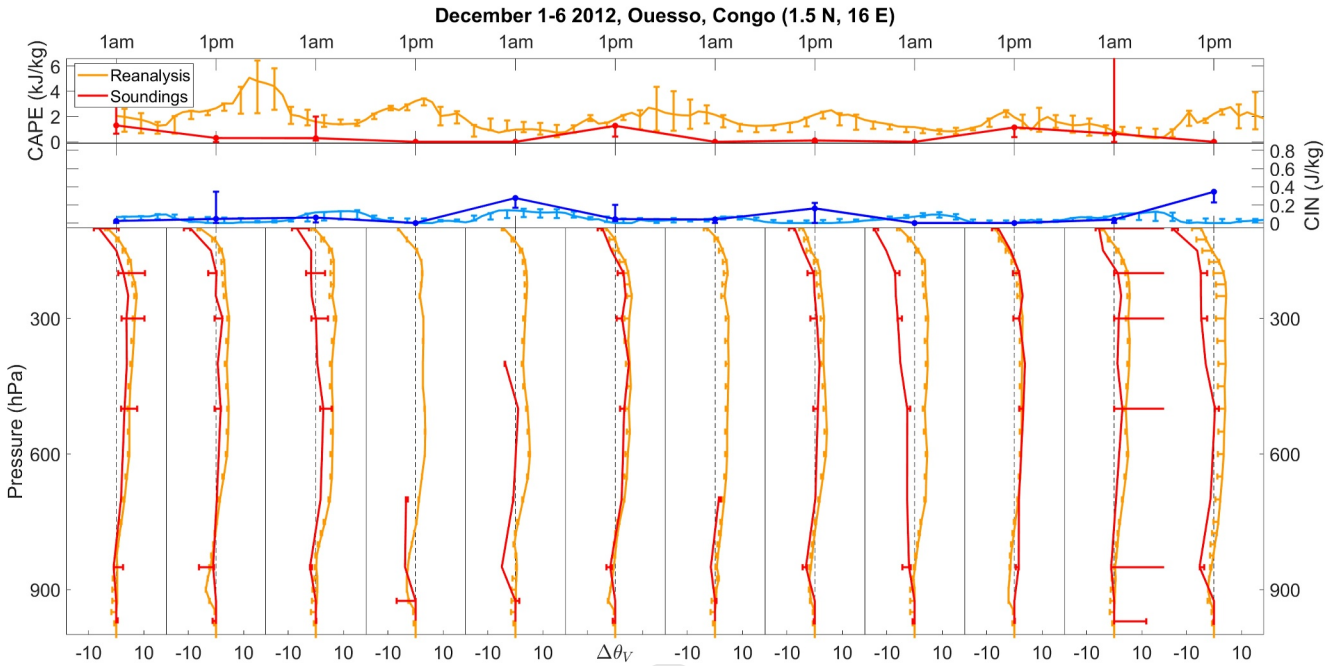

Figure A15. Same as Figure A1 but for Ouesso in the first 6 days of December 2012. The ticks indicate midnight/noon GMT or 1 a.m./p.m. local time. Soundings that do not reach the top of the plot or that have extreme values (December 2nd at 1 p.m., December 3rd at 1 a.m., December 4th at a.m., and December 6 at 1 a.m.) are due to incomplete or unreasonable data.

The first of these is examined in Figure A19. As with previous examples, the temperature matches well between reanalysis and soundings, but the lower level humidity is significantly different. Specifically, a drier lower troposphere leads to decreased $\Delta\theta_V$ in the mid-troposphere.

Our final example sounding is from 4 July 2012 in Ouagadougou (Figure A20). As with previous examples in which the sounding $\Delta\theta_V$ has a large uncertainty, the lower-level humidity is highly variable. Specifically, there is

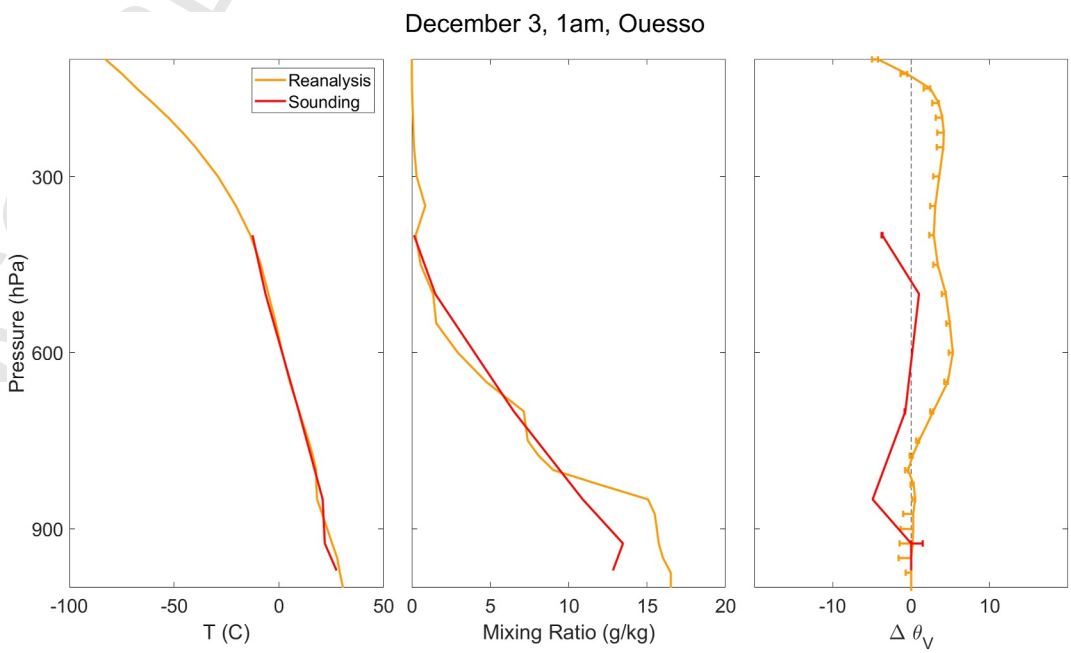

Figure A16. As for Figure A2 but for Ouesso, Congo, on 3 December 2012, at 1 a.m.

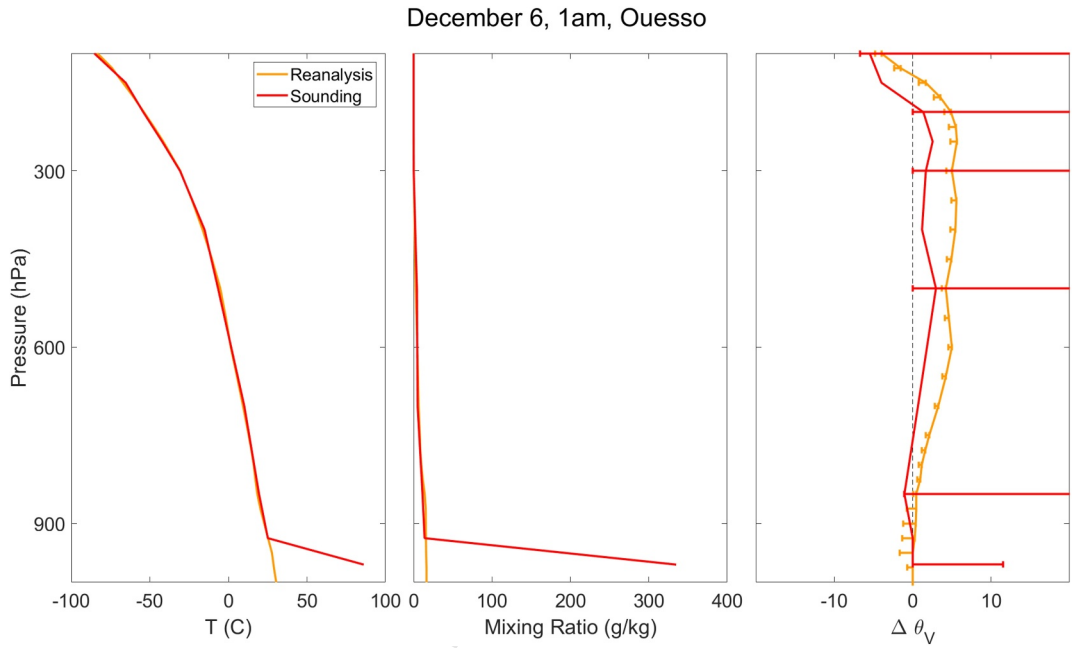

Figure A17. As for Figure A2 but for Ouesso, Congo, on 6 December 2012, at 1 a.m.

a significant increase in humidity at around 950 hPa, and lifting parcels from below this level will lead to a much lower $\Delta\theta_V$ than from above this level. The reanalysis data is much smoother, but even significantly above this level, reanalysis humidity is still lower than that of the sounding. It is unlikely for humidity to be as variable as the sounding indicates on large spatial scales, so it makes sense that reanalysis would be smoother. However, the overall dryness in reanalysis may be due to bias rather than smoothing.

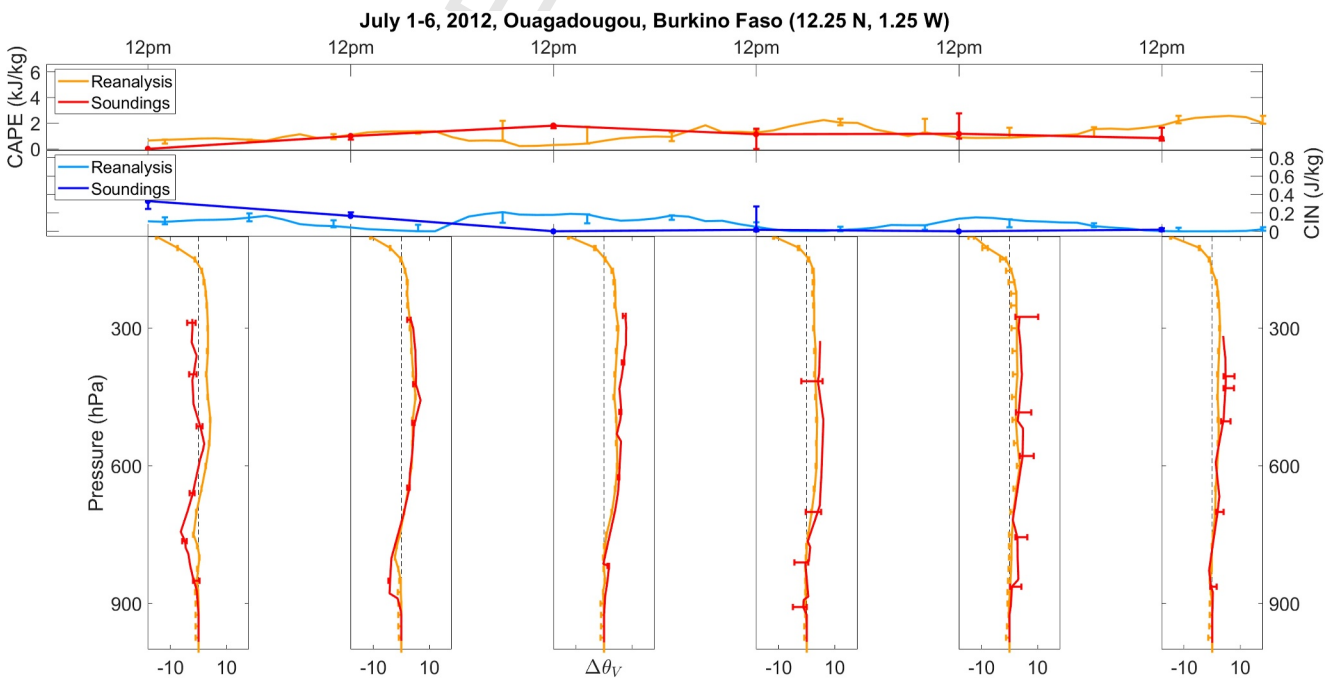

Figure A18. Same as Figure A1 but for Ougadougou in the first 6 days of July 2012. The ticks indicate midnight/noon local time.

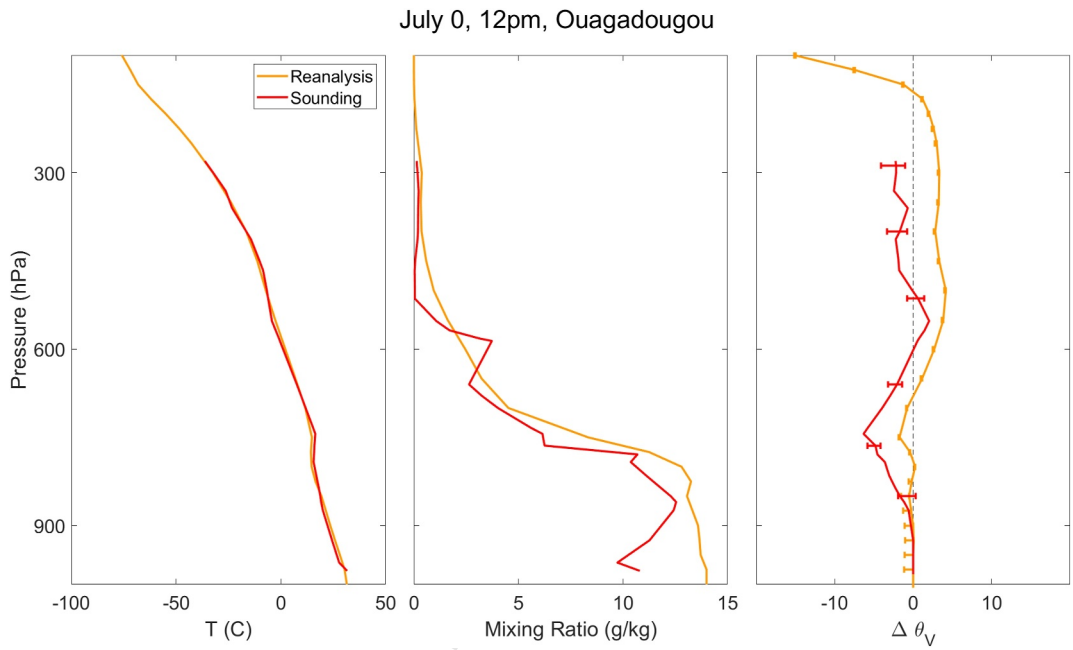

Figure A19. As for Figure A2 but for Ouagadougou, Burkino Faso, on 1 July 2012, at noon.

In summary, most of our sample soundings were a reasonable match for reanalysis. However, in equatorial Africa, data is rare and can give results quite different from reanalysis. Specifically, a significant proportion of the observations we looked at in Ouesso, Congo, did not have uncertainties, which were consistent with ERA5 data. Therefore, we do not believe our Lagrangian method of tracking air properties would be reliable in this region. Specifically, we do not study high CAPE occurrences between 4°N and 15°S in Africa. In other regions, although there are certainly times when reanalysis does not match observations well, these times are relatively rare and likely due to the nature of reanalysis products rather than errors. Therefore, we believe that reanalysis represents the Earth system well enough in most regions to make use of it in the way we have in this work.

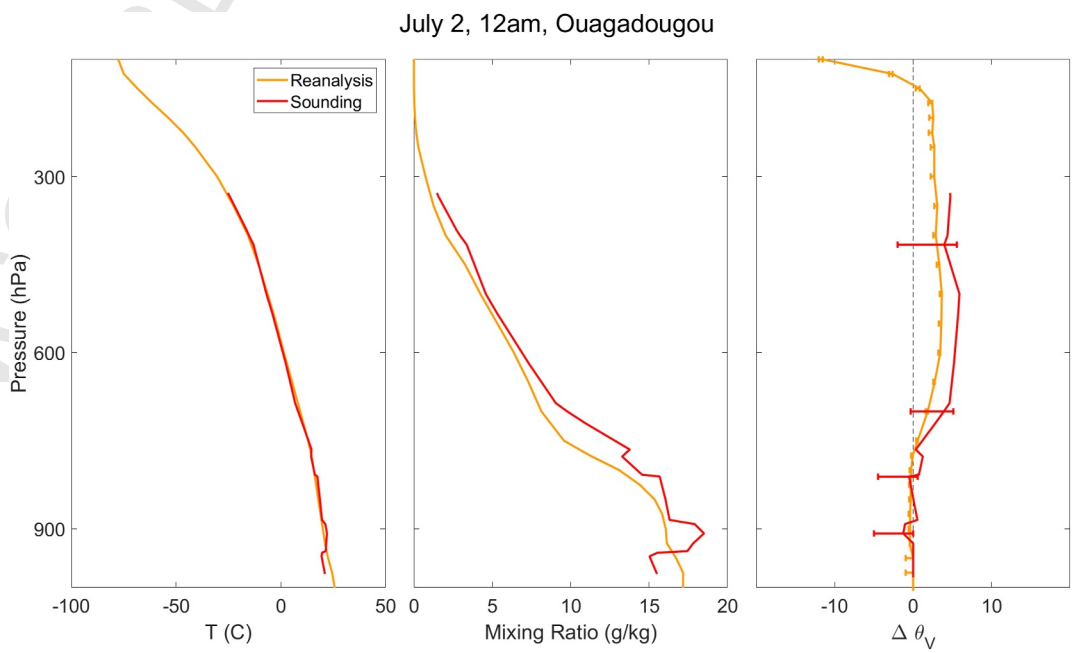

Figure A20. As for Figure A2 but for Ouagadougou, Burkino Faso, on 4 July 2012, at noon.

Data Availability Statement

All reanalysis data used in this study is available from the Copernicus climate data store (https://cds.climate.copernicus.eu/) in the data sets "ERA5 hourly data on pressure levels from 1940 to present" for temperature, humidity, and geopotential, "ERA5 hourly data on single levels from 1940 to present" for the surface fluxes, and "ERA5 monthly averaged data on pressure levels from 1940 to present" for the necessary data to calculate the monthly mean θ_V.

Acknowledgments
P.J. Tuckman is supported by NSF grant OCE-2023520. K. Emanuel was supported by NSF Grant 1906768.

References

Agard, V., & Emanuel, K. (2017). Clausius–Clapeyron scaling of peak CAPE in continental convective storm environments. *Journal of the Atmospheric Sciences*, *74*(9), 3043–3054. https://doi.org/10.1175/JAS-D-16-0352.1

Allen, J. T., Tippett, M. K., & Sobel, A. H. (2015). Influence of the El Niño/Southern Oscillation on tornado and hail frequency in the United States. *Nature Geoscience*, *8*(4), 278–283. https://doi.org/10.1038/ngeo2385

Bluestein, H. B. (2007). Advances in applications of the physics of fluids to severe weather systems. *Reports on Progress in Physics*, *70*(8), 1259–1323. https://doi.org/10.1088/0034-4885/70/8/R01

Botzen, W. J. W., Bouwer, L. M., & van den Bergh, J. C. J. M. (2010). Climate change and hailstorm damage: Empirical evidence and implications for agriculture and insurance. *Resource and Energy Economics*, *32*(3), 341–362. https://doi.org/10.1016/j.reseneeco.2009.10.004

Brooks, H., Doswell, C. A., & Kay, M. P. (2018). Climatological estimates of local daily tornado probability for the United States. *Weather and Forecasting*, *18*(4), 626–640. https://doi.org/10.1175/1520-0434(2003)018⟨0626:CEOLDT⟩2.0.CO;2

Brooks, H. E. (2009). Proximity soundings for severe convection for Europe and the United States from reanalysis data. *Atmospheric Research*, *93*(1), 546–553. https://doi.org/10.1016/j.atmosres.2008.10.005

Brooks, H. E., Lee, J. W., & Craven, J. P. (2003). The spatial distribution of severe thunderstorm and tornado environments from global reanalysis data. *Atmospheric Research*, *67–68*, 73–94. https://doi.org/10.1016/S0169-8095(03)00045-0

Cao, Z. (2008). Severe hail frequency over Ontario, Canada: Recent trend and variability. *Geophysical Research Letters*, *35*(14), L14803. https://doi.org/10.1029/2008GL034888

Carlson, T. N., Benjamin, S. G., Forbes, G. S., & Li, Y.-F. (1983). Elevated mixed layers in the regional severe storm environment: Conceptual model and case studies. *Monthly Weather Review*, *111*(7), 1453–1474. https://doi.org/10.1175/1520-0493(1983)111⟨1453:EMLITR⟩2.0.CO;2

Carlson, T. N., & Ludlam, F. H. (1968). Conditions for the occurrence of severe local storms. *Tellus*, *20*(2), 203–226. https://doi.org/10.1111/j.2153-3490.1968.tb00364.x

Changnon, S. A. (1999). Data and approaches for determining hail risk in the contiguous United States. *Journal of Applied Meteorology and Climatology*, *38*(12), 1730–1739. https://doi.org/10.1175/1520-0450(1999)038⟨1730:DAAFDH⟩2.0.CO;2

Changnon, S. A. (2001). Damaging thunderstorm activity in the United States. *Bulletin of the American Meteorological Society*, *82*(4), 597–608. https://doi.org/10.1175/1520-0477(2001)082⟨0597:DTAITU⟩2.3.CO;2

Changnon, S. A. (2009). Increasing major hail losses in the U.S. *Climatic Change*, *96*(1), 161–166. https://doi.org/10.1007/s10584-009-9597-z

Chaudhuri, S. (2012). Chaotic graph theory approach for identification of convective available potential energy (CAPE) patterns required for the genesis of severe thunderstorms. *Advances in Complex Systems*, *10*(03), 413–422. https://doi.org/10.1142/S0219525907001215

Chen, J., & Dai, A. (2023). The atmosphere has become increasingly unstable during 1979–2020 over the Northern Hemisphere. *Geophysical Research Letters*, *50*(20), e2023GL106125. https://doi.org/10.1029/2023GL106125

Chen, J., Dai, A., Zhang, Y., & Rasmussen, K. (2020). Changes in convective available potential energy and convective inhibition under global warming. *Journal of Climate*, *33*(6), 2025–2050. https://doi.org/10.1175/JCLI-D-19-0461.1

Cook, A. R., Leslie, L. M., Parsons, D. B., & Schaefer, J. T. (2017). The impact of El Niño–Southern Oscillation (ENSO) on winter and early spring U.S. tornado outbreaks. *Journal of Applied Meteorology and Climatology*, *56*(9), 2455–2478. https://doi.org/10.1175/JAMC-D-16-0249.1

Del Genio, A. D., Yao, M.-S., & Jonas, J. (2007). Will moist convection be stronger in a warmer climate? *Geophysical Research Letters*, *34*(16), L16703. https://doi.org/10.1029/2007GL030525

Dessens, J. (1995). Severe convective weather in the context of a nighttime global warming. *Geophysical Research Letters*, *22*(10), 1241–1244. https://doi.org/10.1029/95GL00952

Diffenbaugh, N. S., Scherer, M., & Trapp, R. J. (2013). Robust increases in severe thunderstorm environments in response to greenhouse forcing. *Proceedings of the National Academy of Sciences of the United States of America*, *110*(41), 16361–16366. https://doi.org/10.1073/pnas.1307758110

Doswell, C. A. (1987). The distinction between large-scale and mesoscale contribution to severe convection: A case study example. *Weather and Forecasting*, *2*(1), 3–16. https://doi.org/10.1175/1520-0434(1987)002⟨0003:TDBLSA⟩2.0.CO;2

Doswell, C. A. (2003). Societal impacts of severe thunderstorms and tornadoes: Lessons learned and implications for Europe. *Atmospheric Research*, *67–68*, 135–152. https://doi.org/10.1016/S0169-8095(03)00048-6

Emanuel, K. (2023). On the physics of high CAPE. *Journal of the Atmospheric Sciences*, *80*(11), 2669–2683. https://doi.org/10.1175/JAS-D-23-0060.1

Findell, K. L., & Eltahir, E. A. B. (2003). Atmospheric controls on soil moisture-boundary layer interactions: Three-dimensional wind effects. *Journal of Geophysical Research*, *108*(D8), 8385. https://doi.org/10.1029/2001JD001515

Ford, T. W., Steiner, J., Mason, B., & Quiring, S. M. (2023). Observation-driven characterization of soil moisture-precipitation interactions in the Central United States. *Journal of Geophysical Research: Atmospheres*, *128*(12), e2022JD037934. https://doi.org/10.1029/2022JD037934

Gensini, V. A., & Mote, T. L. (2015). Downscaled estimates of late 21st century severe weather from CCSM3. *Climatic Change*, *129*(1), 307–321. https://doi.org/10.1007/s10584-014-1320-z

Gensini, V. A., Mote, T. L., & Brooks, H. E. (2014). Severe-thunderstorm reanalysis environments and collocated radiosonde observations. *Journal of Applied Meteorology and Climatology*, *53*(3), 742–751. https://doi.org/10.1175/JAMC-D-13-0263.1

Grams, J. S., Thompson, R. L., Snively, D. V., Prentice, J. A., Hodges, G. M., & Reames, L. J. (2012). A climatology and comparison of parameters for significant tornado events in the United States. *Weather and Forecasting*, *27*(1), 106–123. https://doi.org/10.1175/WAF-D-11-00008.1

Groenemeijer, P., & Kühne, T. (2014). A climatology of tornadoes in Europe: Results from the European severe weather database. *Monthly Weather Review*, *142*(12), 4775–4790. https://doi.org/10.1175/MWR-D-14-00107.1

Hersbach, H., Bell, B., Berrisford, P., Hirahara, S., Horányi, A., Muñoz-Sabater, J., et al. (2020). The ERA5 global reanalysis. *Quarterly Journal of the Royal Meteorological Society*, *146*(730), 1999–2049. https://doi.org/10.1002/qj.3803

Hoogewind, K. A., Baldwin, M. E., & Trapp, R. J. (2017). The impact of climate change on hazardous convective weather in the United States: Insight from high-resolution dynamical downscaling. *Journal of Climate*, *30*(24), 10081–10100. https://doi.org/10.1175/JCLI-D-16-0885.1

Johnson, R. H., & Mapes, B. E. (2001). Mesoscale processes and severe convective weather. In C. A. Doswell (Ed.), *Severe convective storms* (pp. 71–122). American Meteorological Society. https://doi.org/10.1007/978-1-935704-06-5_3

Kaplan, J. O., & Lau, K. H.-K. (2021). The WGLC global gridded lightning climatology and time series. *Earth System Science Data*, *13*(7), 3219–3237. https://doi.org/10.5194/essd-13-3219-2021

Krocak, M. J., & Brooks, H. E. (2018). Climatological estimates of hourly tornado probability for the United States. *Weather and Forecasting*, *33*(1), 59–69. https://doi.org/10.1175/WAF-D-17-0123.1

Kunkel, K. E., Karl, T. R., Brooks, H., Kossin, J., Lawrimore, J. H., Arndt, D., et al. (2013). Monitoring and understanding trends in extreme storms: State of knowledge. *Bulletin of the American Meteorological Society*, *94*(4), 499–514. https://doi.org/10.1175/BAMS-D-11-00262.1

Lanicci, J. M., Carlson, T. N., & Warner, T. T. (1987). Sensitivity of the Great Plains severe-storm environment to soil-moisture distribution. *Monthly Weather Review*, *115*(11), 2660–2673. https://doi.org/10.1175/1520-0493(1987)115⟨2660:SOTGPS⟩2.0.CO;2

Li, F., Chavas, D. R., Medeiros, B., Reed, K. A., & Rasmussen, K. L. (2024). Upstream surface roughness and terrain are strong drivers of contrast in tornado potential between North and South America. *Proceedings of the National Academy of Sciences of the United States of America*, *121*(26), e2315425121. https://doi.org/10.1073/pnas.2315425121

Meukaleuni, C., Lenouo, A., & Monkam, D. (2015). Climatology of convective available potential energy (CAPE) in ERA-Interim reanalysis over West Africa. *Atmospheric Science Letters*, *17*(1), 65–70. https://doi.org/10.1002/asl.601

Munday, C., Savage, N., Jones, R. G., & Washington, R. (2023). Valley formation aridifies East Africa and elevates Congo Basin rainfall. *Nature*, *615*(7951), 276–279. https://doi.org/10.1038/s41586-022-05662-5

Murugavel, P., Pawar, S. D., & Gopalakrishnan, V. (2014). Climatology of lightning over Indian region and its relationship with convective available potential energy. *International Journal of Climatology*, *34*(11), 3179–3187. https://doi.org/10.1002/joc.3901

Niall, S., & Walsh, K. (2005). The impact of climate change on hailstorms in southeastern Australia. *International Journal of Climatology*, *25*(14), 1933–1952. https://doi.org/10.1002/joc.1233

Púčik, T., Groenemeijer, P., Rädler, A. T., Tijssen, L., Nikulin, G., Prein, A. F., et al. (2017). Future changes in European severe convection environments in a regional climate model ensemble. *Journal of Climate*, *30*(17), 6771–6794. https://doi.org/10.1175/JCLI-D-16-0777.1

Riemann-Campe, K., Fraedrich, K., & Lunkeit, F. (2009). Global climatology of convective available potential energy (CAPE) and convective inhibition (CIN) in ERA-40 reanalysis. *Atmospheric Research*, *93*(1), 534–545. https://doi.org/10.1016/j.atmosres.2008.09.037

Romps, D. M., Seeley, J. T., Vollaro, D., & Molinari, J. (2014). Projected increase in lightning strikes in the United States due to global warming. *Science*, *346*(6211), 851–854. https://doi.org/10.1126/science.1259100

Schär, C., Lüthi, D., Beyerle, U., & Heise, E. (1999). The soil–precipitation feedback: A process study with a regional climate model. *Journal of Climate*, *12*(3), 722–741. https://doi.org/10.1175/1520-0442(1999)012⟨0722:TSPFAP⟩2.0.CO;2

Schneider, R., & Dean, A. (2008). A comprehensive 5-year severe storm environment climatology for the continental United States. Retrieved from https://origin-west-www-spc.woc.noaa.gov/publications/schneider/5yr-clim.pdf

Schultz, D. M., Richardson, Y. P., Markowski, P. M., & Doswell, C. A. (2014). Tornadoes in the Central United States and the "Clash of Air Masses". *Bulletin of the American Meteorological Society*, *95*(11), 1704–1712. https://doi.org/10.1175/BAMS-D-13-00252.1

Seeley, J. T., & Romps, D. M. (2015). The effect of global warming on severe thunderstorms in the United States. *Journal of Climate*, *28*(6), 2443–2458. https://doi.org/10.1175/JCLI-D-14-00382.1

Sherburn, K. D., & Parker, M. D. (2014). Climatology and ingredients of significant severe convection in high-shear, low-CAPE environments. *Weather and Forecasting*, *29*(4), 854–877. https://doi.org/10.1175/WAF-D-13-00041.1

Taszarek, M., Allen, J., Marchio, M., & Brooks, H. (2021). Global climatology and trends in convective environments from ERA5 and rawinsonde data. *Climate and Atmospheric Science*, *4*(1), 35. https://doi.org/10.1038/s41612-021-00190-x

Taszarek, M., Brooks, H. E., Czernecki, B., Szuster, P., & Fortuniak, K. (2018). Climatological aspects of convective parameters over Europe: A comparison of ERA-Interim and sounding data. *Journal of Climate*, *31*(11), 4281–4308. https://doi.org/10.1175/JCLI-D-17-0596.1

Taszarek, M., Pilguj, N., Allen, J., Gensini, V., Brooks, H., & Szuster, P. (2021). Comparison of convective parameters derived from ERA5 and MERRA-2 with rawinsonde data over Europe and North America. *Journal of Climate*, *34*(8), 3211–3237. https://doi.org/10.1175/JCLI-D-20-0484.1

Taylor, C., & Ellis, R. (2006). Satellite detection of soil moisture impacts on convection at the mesoscale. *Geophysical Research Letters*, *33*(3), L03404. https://doi.org/10.1029/2005GL025252

Trapp, R. J., Diffenbaugh, N. S., Brooks, H. E., Baldwin, M. E., Robinson, E. D., & Pal, J. S. (2007). Changes in severe thunderstorm environment frequency during the 21st century caused by anthropogenically enhanced global radiative forcing. *Proceedings of the National Academy of Sciences of the United States of America*, *104*(50), 19719–19723. https://doi.org/10.1073/pnas.0705494104

Trapp, R. J., & Hoogewind, K. A. (2016). The realization of extreme tornadic storm events under future anthropogenic climate change. *Journal of Climate*, *29*(14), 5251–5265. https://doi.org/10.1175/JCLI-D-15-0623.1

Tuckman, P., Agard, V., & Emanuel, K. (2023). Evolution of convective energy and inhibition before instances of large CAPE. *Journal of Climate*, *151*(1), 321–338. https://doi.org/10.1175/MWR-D-21-0302.1

Weisman, M. L., & Klemp, J. B. (1982). The dependence of numerically simulated convective storms on vertical wind shear and buoyancy. *Monthly Weather Review*, *110*(6), 504–520. https://doi.org/10.1175/1520-0493(1982)110⟨0504:TDONSC⟩2.0.CO;2

Westermayer, A., Groenemeijer, P., Pistotnik, G., Sausen, R., & Faust, E. (2017). Identification of favorable environments for thunderstorms in reanalysis data. *Meteorologische Zeitschrift*, *26*(1), 59–70. https://doi.org/10.1127/metz/2016/0754

Xu, K.-M., & Emanuel, K. A. (1989). Is the tropical atmosphere conditionally unstable? *Monthly Weather Review*, *117*(7), 1471–1479. https://doi.org/10.1175/1520-0493(1989)117⟨1471:ITTACU⟩2.0.CO;2

Yang, G., & Shu, C. (1985). Large-scale environmental conditions for thunderstorm development. *Advances in Atmospheric Sciences*, *2*(4), 508–521. https://doi.org/10.1007/BF02678749

Zhang, L., Gianotti, D., & Entekhabi, D. (2023). Land surface influence on convective available potential energy (CAPE) change during interstorms. *Journal of Hydrometeorology*, *24*(8), 1365–1376. https://doi.org/10.1175/JHM-D-22-0191.1

Zipser, E. J., Cecil, D. J., Liu, C., Nesbitt, S. W., & Yorty, D. P. (2006). Where are the most intense thunderstorms on Earth? *Bulletin of the American Meteorological Society*, *87*(8), 1057–1072. https://doi.org/10.1175/BAMS-87-8-1057